Large Scale Structure Observations*

Will J. Percival

Institute of Cosmology and Gravitation, University of Portsmouth,

Dennis Sciama Building, Portsmouth, P01 3FX, UK

Abstract

Galaxy Surveys are enjoying a renaissance thanks to the advent of multi-object spectrographs on ground-based telescopes. The last 15 years have seen the fruits of this experimental advance, including the 2-degree Field Galaxy Redshift Survey (2dFGRS; Colless *et al.* 2003) and the Sloan Digital Sky Survey (SDSS; York *et al.* 2000). Most recently, the Baryon Oscillation Spectroscopic Survey (BOSS; Dawson *et al.* 2013), part of the SDSS-III project (Eisenstein *et al.* 2011), has provided the largest volume of the low-redshift Universe ever surveyed with a galaxy density useful for high-precision cosmology. This set of lecture notes looks at some of the physical processes that underpin these measurements, the evolution of measurements themselves, and looks ahead to the next 15 years and the advent of surveys such as the enhanced Baryon Oscillation Spectroscopic Survey (eBOSS), the Dark Energy Spectroscopic Instrument (DESI) and the ESA Euclid satellite mission.

Contents

---

1   Clustering statistics

1.1   The over-density field

Any galaxy survey will observe a particular "window" of the Universe, consisting of an angular mask of the area observed, and a radial distribution of galaxies. In order to correct for a spatially varying galaxy selection function, we translate the observed galaxy density $\rho(\mathbf{x})$ to a dimensionless over-density

$$\delta(\mathbf{x}) = \frac{\rho(\mathbf{x}) - \bar{\rho}(\mathbf{x})}{\bar{\rho}(\mathbf{x})}, \tag{1}$$

where $\bar{\rho}(\mathbf{x})$ is the expected mean density.

At early times, or on large-scales, $\delta(\mathbf{x})$ has a distribution that is close to that of Gaussian, adiabatic fluctuations (Planck Collaboration *et al.* 2013*a*), and thus the statistical distribution is completely described by the two-point functions of this field.

1.2   The correlation function

The correlation function is the expected 2-point function of this statistic

$$\xi(\mathbf{x_1}, \mathbf{x_2}) \equiv \langle \delta(\mathbf{x_1}) \delta(\mathbf{x_2}) \rangle. \tag{2}$$

From statistical homogeneity and isotropy, we have that

$$\begin{aligned} \xi(\mathbf{x_1}, \mathbf{x_2}) &= \xi(\mathbf{x_1} - \mathbf{x_2}), \\ &= \xi(|\mathbf{x_1} - \mathbf{x_2}|). \end{aligned} \tag{3}$$

To help understand the correlation function, suppose that we have two small regions, δV_1 and δV_2, separated by a distance r. Then the expected number of pairs of galaxies with one galaxy in δV_1 and the other in δV_2 is given by

$$\langle n_{\mathrm{pair}} \rangle = \bar{n}^2 \left[1 + \xi(r) \right] \delta V_1 \delta V_2 \,, \tag{4}$$

where $\bar{n}$ is the mean number of galaxies per unit volume. We see that $\xi(r)$ measures the excess clustering of galaxies at a separation r. Imagine throwing down a large number of randomly placed, equal length r, "sticks" within a survey. Then the correlation function for that separation r is the excessive fraction of sticks with a galaxy close to both ends, compared with sticks that have randomly chosen points within the survey window close to both ends.

If $\xi(r) = 0$, the galaxies are unclustered (randomly distributed) on this scale – the number of pairs is just the expected number of galaxies in δV_1 times the expected number in δV_2. Here, the same number of "sticks" have close-galaxies at both ends, compared with randomly chosen points within the survey window. $\xi(r) > 0$ corresponds to strong clustering, and $\xi(r) < 0$ to anti-clustering. The estimation of $\xi(r)$ from a sample of galaxies will be discussed in Section 4.4.

1.3 The power spectrum

It is often convenient to measure clustering in Fourier space. In cosmology the following Fourier transform convention is most commonly used

$$\delta(\mathbf{k}) \quad = \quad \int \delta(\mathbf{r}) e^{i\mathbf{k}.\mathbf{r}} d^3 r \,, \tag{5}$$

$$\delta(\mathbf{r}) \quad = \quad \int \delta(\mathbf{k}) e^{-i\mathbf{k}.\mathbf{r}} \frac{d^3 k}{(2\pi)^3} \,. \tag{6}$$

The power spectrum is defined as

$$P(\mathbf{k_1}, \mathbf{k_2}) = \frac{1}{(2\pi)^3} \langle \delta(\mathbf{k_1}) \delta(\mathbf{k_2}) \rangle \,, \tag{7}$$

with statistical homogeneity and isotropy giving

$$P(\mathbf{k_1}, \mathbf{k_2}) = \delta_D(\mathbf{k_1} - \mathbf{k_2}) P(k_1) \,, \tag{8}$$

where δ_D is the Dirac delta function. The correlation function and power spectrum form a Fourier pair

$$P(k) \quad = \quad \int \xi(r) e^{i\mathbf{k}.\mathbf{r}} d^3 r \,, \tag{9}$$

$$\xi(r) \quad = \quad \int P(k) e^{-i\mathbf{k}.\mathbf{r}} \frac{d^3 k}{(2\pi)^3} \,, \tag{10}$$

so they provide the same information. The choice of which to use is therefore somewhat arbitrary (see Hamilton 2005 for a further discussion of this). In order to understand the power spectrum, we need to think about "throwing down" Fourier waves, rather than sticks, but the principle is the same. Methods to calculate the power spectrum from a sample of galaxies are considered in Section 4.3.

3

1.4 Higher order statistics

The extension of the 2-pt statistics, the power spectrum and the correlation function, to higher orders is straightforward, with Eq. 4 becoming

$$\langle n_{\text{tuple}} \rangle = \bar{n}^n \left[1 + \xi^{(n)} \right] \delta V_1 \cdots \delta V_n \,. \tag{11}$$

However, as we will discuss in Section 1.3, at early times and on large scales, we expect the over-density field to have Gaussian statistics. This follows from the central limit theorem, which implies that a density distribution is asymptotically Gaussian in the limit where the density results from the average of many independent processes. The over-density field has zero mean by definition so, in this regime, is completely characterised by either the correlation function or the power spectrum. Consequently, measuring either the correlation function or the power spectrum provides a statistically complete description of the field. Higher order statistics tell us about the break-down of the linear regime, showing how the gravitational build-up of structures occurs and allowing tests of General Relativity.

1.5 Anisotropic statistics

Although the true Universe is expected to be statistically homogeneous and isotropic, the observed Universe is not so, because of a number of observational effects discussed in Section 5. Statistically, these effect are symmetric around the line-of-sight and, in the distant-observer limit possess a reflectional symmetry along the line-of-sight looking outwards or inwards. Thus, to first order, the anisotropies in the over-density field can be written as a function of μ^2, where μ is the cosine of the angle to the line-of-sight. Consequently, we often write the correlation function $\xi(r, \mu)$ and the power spectrum $P(k, \mu)$.

It is common to expand both the correlation function and power spectrum in Legendre polynomials $L_\ell(\mu)$ to give multipole moments,

$$P_\ell(k) \equiv \frac{2\ell + 1}{2} \int_{-1}^{+1} d\mu \, P(k, \mu) \, L_\ell(\mu) \,. \tag{12}$$

The first three even Legendre polynomials are $L_0(\mu) = 1$, $L_2(\mu) = (3\mu^2 - 1)/2$ and $L_4(\mu) = (35\mu^4 - 30\mu^2 + 3)/8$.

2 The comoving matter power spectrum

The present-day matter power spectrum is the evolved result of the primordial power spectrum produced during inflation, a period of rapid acceleration in the early Universe. Inflation explains why apparently causally disconnected regions have similar properties, and why the energy-density is close to the critical value, as well as explaining the existence of present-day structure. While the general paradigm of inflation is widely accepted, the details are largely unconstrained (see Byrnes and Choi 2010). Although we know that the post-inflation distribution of fluctuations has a statistical distribution close to a Gaussian (Planck Collaboration *et al.* 2013*a*), determining the amount of non-Gaussianity provides a key way of distinguishing between models.

The post-inflation matter power spectrum is commonly parameterised by a power law, $P(k) \propto k^n$, where the power-law index $n = 0.96$ (Planck Collaboration *et al.* 2013*b*). This power spectrum is subsequently altered by physical process within the evolving Universe composed of radiation, baryons, neutrinos, dark matter and dark energy. In particular, the relative densities of

these components changes with scale factor a according to the Friedman equation, which for a ΛCDM Universe can be written in the form

$$E^2(a) \equiv \frac{H^2(a)}{H_0^2} = \Omega_R a^{-4} + \Omega_M a^{-3} + \Omega_k a^{-2} + \Omega_\Lambda \,, \tag{13}$$

where $E(a)$ is the Hubble Parameter $H(a)$ normalised to its present day value, Ω_R, Ω_M, and Ω_Λ are the present-day radiation, matter and Λ densities in units of the critical density, and Ω_k is the spatial curvature density ($= 1 - \Omega_{\rm tot}$). a is the cosmological scale factor, $a = 1/(1 + z)$, such that this equation and the parameters within can be written as functions of either a or z. The physics, including the important processes that are described in the following subsections, is usually encoded in a transfer function $T(k)$, which details the change in the power spectrum from the inflationary form through to the power spectrum in the matter dominated regime (the regime where the dominant term in Eq. 13 is $\Omega_M a^{-3}$).

2.1 The matter-radiation equality scale

The growth of dark matter fluctuations is intimately linked to the Jeans scale. Perturbations smaller than the Jeans scale do not collapse due to pressure support – for collision-less dark matter this means being supported by internal random velocities. Perturbations larger than the Jeans scale grow through gravity at the same rate, independent of scale. If we approximate the Universe as containing just dark matter and radiation, the Jeans scale grows to the size of the horizon at matter-radiation equality, and then reduces to zero when the matter dominates. We therefore see that the horizon scale at matter-radiation equality will be imprinted in the distribution of fluctuations – this scale marks a turn-over in the growth rate of fluctuations. What this means in practice is that there is a cut-off in the power spectrum on small scales, dependent on $\Omega_M h^2$. When this scale is observed in a low-redshift galaxy power spectrum, its position is dependent on $\Omega_M h$, where $h = H_0/100\,{\rm km\,s}^{-1}\,{\rm Mpc}^{-1}$, as projection effect introduce another factor of h.

2.2 Neutrino masses

The same principal of gravitational collapse versus pressure support can be applied in the case of massive neutrinos. Initially the neutrinos are relativistic and their Jeans scale grows with the horizon. As their temperature decreases their momenta drop, they become non-relativistic, and the Jeans scale decreases – they can subsequently fall into perturbations. Massive neutrinos are interesting because even at low redshifts the Jeans scale is cosmologically relevant. Consequently the linear power spectrum (the fluctuation distribution excluding the non-linear collapse of perturbations) is not frozen shortly after matter-radiation equality. Instead its form is still changing at low redshifts. Additionally, the growth rate depends on the scale - it is suppressed until neutrinos collapse into perturbations, simply because the perturbations have lower amplitude.

Both the imprint of the matter-radiation equality scale and neutrino masses are further complicated by galaxy bias (see Section 3.4), which limits measurements made from galaxy surveys. However, cosmological neutrino mass measurements are still of strong interest as the standard model of particle physics links together cosmological photon and neutrino species densities: based on current photon density (as measured from the CMB), we expect a cosmological neutrino background with a density $112\,{\rm cm}^{-3}$ per species, which leads to an expected cosmological density

$$f_\nu = \frac{\Omega_\nu}{\Omega_M} = \frac{\sum m_\nu}{93\Omega_M h^2\,{\rm eV}} \,. \tag{14}$$

Thus a measurement of the cosmological density directly gives a measurement of the summed neutrino mass, and has the potential to provide information on the mass hierarchy: Neutrinos come in three flavours, and detectors measure differences among the three mixed states, but the masses themselves are unknown. An interesting question is whether the biggest difference marks the heaviest mixed state (the so-called normal hierarchy) or the lightest one (an inverted hierarchy).

2.3 Baryons

At early epochs baryons are coupled to the photons and are subject to radiation pressure. If we consider a single fluctuation existing after inflation, then a spherical shell of baryonic material and photons is driven away from the perturbation by this pressure. When the photons and gas decouple, a spherical shell of baryons is left around a central concentration of dark matter. As the perturbation evolves through gravity, the density profiles of the baryons and dark matter grow together, and the final perturbation profile is left with a small increase in density in a spherical shell at a radial location corresponding to the sound horizon at the end of the Compton drag epoch r_d: this is the radius of the spherical shell (Bashinsky and Bertschinger 2001; Bashinsky and Bertschinger 2002). In order to understand the effect of this process on a field of perturbations, one can imagine many of these superimposed "waves" propagating simultaneously, resulting in a slight preference for perturbations separated by the scale of the sound horizon (perturbations at the original location, and at the spherical shell). When translated into the power spectrum, this becomes a series of oscillations in the same way that the Fourier transform of a top-hat function is a Sinc function.

In addition to these features (called Baryon Acoustic Oscillations, or BAO), fluctuations smaller than the Jeans scale, which tracks the sound horizon until decoupling, do not grow, while large fluctuations are unaffected and continue to grow. The presence of baryons therefore also leads to a reduction in the amplitude of small scale fluctuations. A description of the physics for baryons is given by Eisenstein and Hu (1998) or Appendix A of Meiksin *et al.* (1999), and a discussion of the acoustic signal in configuration space can be found in Eisenstein *et al.* (2007*b*).

In an evolved density field at low redshifts, BAO are damped on small scales due to large-scale bulk flows, which are well described as being random (Eisenstein *et al.* 2007*a*). If we write the original power spectrum as $P_{\rm lin}(k)$, and a version without BAO as $P_{\rm nw}(k)$, then

$$P(k) = P_{\rm lin}(k)e^{-\frac{k^2\sigma^2}{2}} + P_{\rm nw}(k)\left(1 - e^{-\frac{k^2\sigma^2}{2}}\right), \tag{15}$$

where σ controls the amplitude of the damping. The observed damping is expected to be stronger along the line-of-sight due to the contribution from Redshift-Space Distortions (see Section 5.2).

3 Physical Processes

We saw in the previous section that the large-scale distribution of perturbations in the matter field has the potential to provide a wealth of cosmological information, as it encodes a number of different physical processes. When we observe the field by means of a galaxy survey, we see the evolved product of the linear field, as traced by galaxies. The differences between the galaxy field and the original linear matter perturbations can be understood using a number of simple models that help to explain how the build-up of structure leads to galaxy formation.

3.1 Linear structure growth

The simplest model for cosmological structure growth follows from Birkhoff's theorem, which states that a spherically symmetric gravitational field in empty space is static and is always described by the Schwarzchild metric (Birkhoff and Langer 1923). Thus, a homogeneous sphere of uniform density with radius a_p (subscript p refers to the perturbation) can itself be modelled using the same equations that govern the evolution of the Universe, with scale factor a. From this we can derive the linear growth rate (e.g. Peebles 1980). We assume that we have two spheres containing the same mass, one of background density ρ, and one with density ρ_p, where

$$\rho_p a_p^3 = \rho a^3, \ \ \delta \equiv \rho_p/\rho - 1 \, , \tag{16}$$

giving, to first order in δ, $a_p = a(1 - \delta/3)$. The cosmological equation for both the spherical perturbation and the background is

$$\frac{1}{a}\frac{d^2a}{dt^2} = -H_0^2 \left[\frac{1}{2}\Omega_M a^{-3} - \Omega_\Lambda \right] \, , \tag{17}$$

where a should be replaced by a_p in the matter density term for the perturbation, and we assume a ΛCDM background model. Using this equation for both spheres, and substituting in the linear equation for δ as a function of a and a_p gives, to first order

$$\frac{3}{2}\Omega_M(a) = \frac{d^2\ln\delta}{d\ln a^2} + \left(\frac{d\ln\delta}{d\ln a} \right)^2 + \frac{d\ln\delta}{d\ln a}\left\{ 1 - \frac{1}{2}\Omega_M(a) - \Omega_\Lambda \right\} \, , \tag{18}$$

where we have simplified this equation by including the evolution of the matter and Λ densities with respect to the critical density,

$$\Omega_M(a) = \frac{\Omega_M a^{-3}}{E^2(a)}, \ \ \Omega_\Lambda(a) = \frac{\Omega_\Lambda}{E^2(a)} \, . \tag{19}$$

$E(a)$ was given in Eq. 13. This simple derivation, and the solutions to this equation $\delta(z) \propto G(z)$, where $G(z)$ is the linear growth rate, show how large-scale densities grow within the background Universe. More details of this derivation, and a formula valid for general non-interacting Dark Energy models, are given in Percival (2005).

3.2 Spherical collapse

In the above subsection, we saw how the evolution of spherical perturbations follows that of *mini-Universes*, with different initial densities. A first-order solution was presented, giving the linear growth rate $G(z)$. Going beyond the first order, the evolution of the perturbations can be followed further, until the effects of the assumption of homogeneity become apparent. Closed cosmological models, which are analogous to collapsed objects, start with sufficient density that the gravitational attraction overcomes Dark Energy leading to eventual collapse. Open cosmological models, which are analogous to under-dense regions, start with so little density that gravity cannot influence the initial expansion.

Fig. 1 shows the evolution of the perturbation scale for various initial conditions, and the link to the linear growth of perturbation scale. Given a low initial density, such as expected for a "void", the perturbation will expand more rapidly than the background, whereas more dense regions, such as large groups of galaxies, collapse. Within this simple model, collapse to a singularity is predicted; in practice the granulation of material leads to virialisation at a fixed radius.
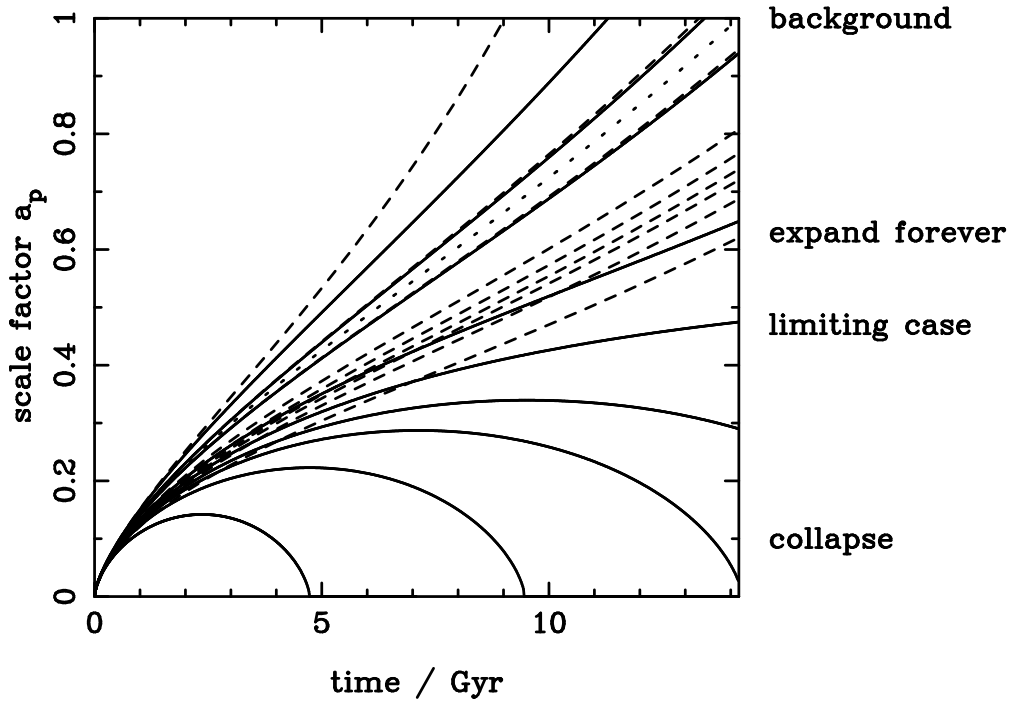
Figure 1: The evolution of the perturbation scale factor a_p, as a function of the local density of the patch of universe under consideration (solid lines). These were calculated for a flat ΛCDM cosmology, with $\Omega_M = 0.25$. The dashed lines show the linear extrapolation of the initial perturbation over-density. The dotted line shows the background expansion. Within the simple spherical collapse model, sufficiently over-dense regions collapse to singularities, while under-dense regions expand forever. The relationship between the linear growth of perturbations (discussed in Section 3.1), and the non-linear evolution (discussed in Section 3.2) can clearly be seen by comparing solid and dashed lines.

At any epoch, there is a critical initial density for collapse: perturbations that are more dense have collapsed by the epoch of interest, while less dense perturbations have not. For ease, the critical density is usually extrapolated using linear theory to present-day, and is called the linearly-extrapolated critical density for collapse δ_c. δ_c has a weak dependence on cosmological model, and a review of methods to calculate δ_c is given in, for example, Percival (2005). Given the weak dependence it is commonly approximated by its value for an Einstein-de Sitter cosmological model

$$\delta_c \simeq 1.686 \frac{G(0)}{G(z)} \,, \tag{20}$$

where $G(z)$ is the standard linear growth rate, which extrapolates the initial over-density to present day.

3.3 Press-Schechter theory

Taking the spherical model one step further it is possible to form a "complete", although simplistic, model for structure growth as a function of the mass of an object. Press and Schechter (1974) introduced the concept of smoothing the initial density field to determine the relative abundances of perturbations with different mass. For a filter of width R, corresponding to a mass scale $M = 4/3\pi\rho R^3$ where ρ is the average density of the Universe, smoothing the matter field with power spectrum $P(k)$ gives a further field with spatial variance

$$\sigma_M^2 = \frac{1}{2\pi} \int_0^\infty P(k) W^2(k,R) k^2 \, dk \,, \tag{21}$$

where $W(k,R)$ is the window function for the smoothing. If a sharp k-space filter is used then, around any spatial location, the smoothed over-density forms a Brownian random walk in δ, as a function of filter radius (usually plotted as σ_M^2). Comparing the relative numbers of trajectories that have crossed the critical density (as discussed in the previous section) at a mass greater than that of interest (some may cross at high mass, but be below the critical density at low mass, but still be counted as collapsed objects), gives a distribution of haloes with mass (commonly called a "mass function")

$$f(>M) = 2 \int_{\delta_c}^\infty \frac{\delta_c}{\sqrt{2\pi\sigma_M^2}} \exp\left(-\frac{\delta^2}{2\sigma_M^2}\right) d\delta \,. \tag{22}$$

Thus we have a complete model for structure formation: smoothing the fluctuations leads to the masses of collapsed objects, while the spherical perturbation model gives the epoch of collapse for those perturbations that are sufficiently dense. Comparing with numerical simulations reveals that, while this is a good model, it cannot accurately predict the measured redshift-dependent mass function, and fitting formulae to N-body simulations are the currently preferred way to model this (e.g. Sheth and Tormen 1999; Jenkins *et al.* 2001).

3.4 Galaxy bias

The above discussion only considered concentrations of mass, which are commonly referred to as "haloes", whereas the most easily observed extragalactic objects are galaxies. In general, a sample of galaxies will form a Poisson sampling of some underlying field with over-density δ_g, but this field may be different from the matter field, which has over-density δ_M. Here, a subscript g refers to galaxies, and M to the matter. This "bias" between fields encodes the physics of galaxy formation, and may therefore be a general, non-local, non-linear function. On large-scales we will now see that this bias reduces to a local, linear function $b \equiv \delta_g/\delta_M$.

The simplest model for large-scale galaxy bias is the peak-background split model (Bardeen *et al.* 1986; Cole and Kaiser 1989). Here it is postulated that halo formation depends on the local density field δ_M. Large scale density modes δ_l can alter the local halo density n by pushing pieces of the density field above a critical threshold, leading to a change in the number density of haloes,

$$n \rightarrow n - \frac{dn}{d\delta_c}\delta_l \, . \tag{23}$$

To first order, the addition of the long wavelength mode leads to a bias,

$$b \equiv \frac{\delta_{\text{new}}}{\delta_l} = 1 - \frac{d\ln n}{d\delta_c} \, , \tag{24}$$

where δ_{new} is the boosted over-density. Thus we see how the shape of the mass function gives the large-scale (linear) bias of haloes. On large scales we expect a linear relationship between the large scale mode amplitudes and the change in number density, so the shape of the galaxy and mass power spectra are the same.

Fig. 2 shows the result of the peak-background split model, giving the amplitude of clustering for haloes of different mass as a function of redshift. Higher mass haloes have stronger clustering as a result of the steeper mass function, which means that a small long-wavelength perturbation can have a disproportionate effect on the number density of haloes.

On small scales, the peak-background split model no longer holds, and we must look to other models for the clustering of galaxies. One such model is the "halo" model (Seljak 2000; Peacock and Smith 2000; Cooray and Sheth 2002), which is a simple framework where galaxies trace halos on large scales, with bias determined by the distribution of halo masses within which the galaxies reside. On small scales, we expect galaxy clustering to be different from that of the halos, as pairs of galaxies inside single collapsed structures become important. The halo model simply combines these two scenarios into a full-scale model for galaxies.

4 Galaxy Survey basics

In this section we explore some of the practical ideas and methods used to analyse a galaxy survey and make cosmological measurements. The clustering signal is a 3-dimensional signal, so ideally we wish to know the distribution of matter (or galaxies) in 3D. However, while the angular positions of galaxies are in general easy to measure, the radial distances are not so easy. In order to estimate distances to galaxies, large surveys typically use the spectrum of light emitted by galaxies, including absorption and emission lines and more general features, all resulting from the integrated stellar light. By comparing these features to rest-frame models, the redshifts of the galaxies can be estimated and, using the Hubble expansion rate, their distances.

It is possible to fit observed broad-band colours with templates or training samples of emitted light profiles, and thus estimate galaxy recession velocities. These "photometric redshifts" - redshifts estimated from broad-band colours only - vary in quality between galaxy samples. For example, they can have offsets from the true redshifts with standard deviations of $\sim 0.03(1+z)$ for red galaxies with strong 4000 Å breaks (Ross *et al.* 2011), while more general populations can give estimates with $\sigma_z \sim 0.05(1+z)$. The level of precision depends on the photometric quality of the data used, the number of bands, etc. If spectra can be obtained for galaxies, then absorption and emission lines can be used to estimate redshifts with typical errors of $\sim 0.001...0.0001(1+z)$, allowing clustering along the line-of-sight to be more accurately measured.
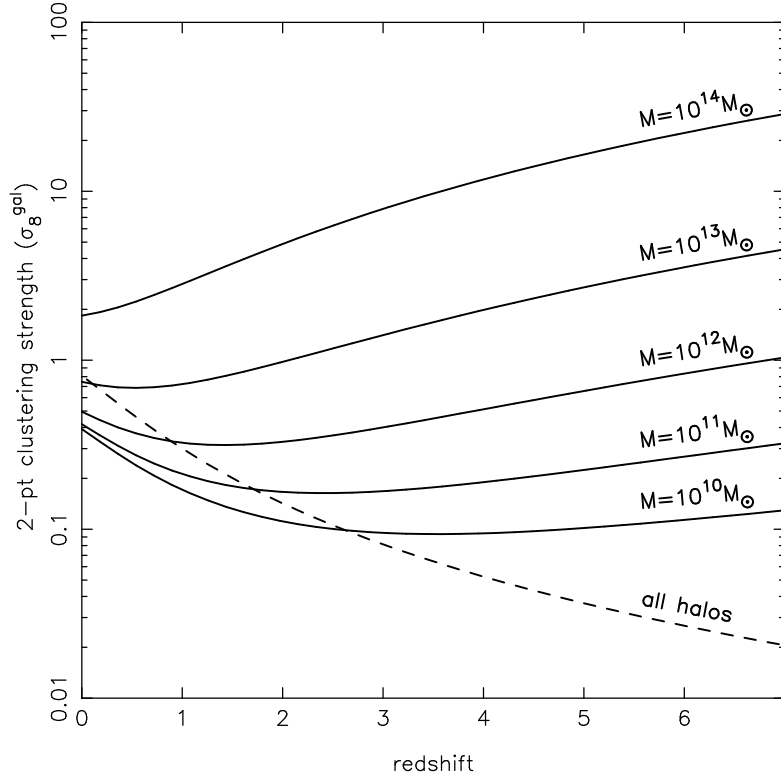
Figure 2: The expected large-scale clustering amplitude for haloes of different mass as a function of scale, compared to the linear growth rate. Clustering has been estimated using the peak-background split model for a standard ΛCDM cosmological model. Haloes are expected to grow in mass with time, so will not evolve along the lines shown, which link objects of the same mass at different times. The dashed line shows the expected growth in the clustering of all of the mass, as given by $G(z)$.

4.1 Overview of galaxy surveys

Recent advances in galaxy surveys have largely been driven by new instrumentation that enables multiple galaxy spectra to be obtained simultaneously. Using these multi-object spectrographs (MOS), a number of survey teams have created maps of many hundreds of thousands or millions of galaxies. Key wide-field facilities include the AAΩ instrument on the Anglo-Australian Telescope, which has been used to conduct the 2-degree Field Galaxy Redshift Survey (2dF-GRS; Colless *et al.* 2003) and Wigglez (Drinkwater *et al.* 2010) surveys, and the Sloan Telescope, which has been used for the Sloan Digital Sky Survey (SDSS; York *et al.* 2000).

In following sections we will use results from the Baryon Oscillation Spectroscopic Survey (BOSS Dawson *et al.* 2013), part of the SDSS-III project (Eisenstein *et al.* 2011) to demonstrate possible measurements. BOSS is primarily a spectroscopic survey, which is designed to obtain spectra and derive redshifts from them for 1.2 million galaxies over an extragalactic footprint covering 10 000 square degrees. 1000 spectra are simultaneously recovered in each observation, using aluminium plates with drilled holes to locate manually plugged optical fibres that feed a pair of double spectrographs. Each observation is performed in a series of 900-second exposures, integrating until a minimum signal-to-noise ratio is achieved for the faint galaxy targets. The resulting data set has high redshift completeness > 97 per cent over the full survey footprint.

4.2 Measuring over-densities

As described in Section 1.1, we need to translate from an observed galaxy density to a dimensionless over-density. For a galaxy survey, this means understanding where you could have observed galaxies (called the survey *mask*), not just where galaxies were observed. For current surveys, the mask can be split into independent radial and angular components, where the angular component of the mask includes the varying completeness and purity of observations and the radial component depends on the galaxy selection criteria. For a magnitude-limited catalogue, the radial distribution can be determined by integrating under a model luminosity function (Cole 2011), while for a colour selected sample, a fit to the galaxy distribution is usually performed (Anderson *et al.* 2012). The mask is commonly quantified by means of a random catalogue - a catalogue of spatial positions that Poisson sample the expected density $\bar{\rho}$ (see Eq. 1), as outlined by the mask. This catalogue has the same spatial selection function as the galaxies but no clustering.

If the correct mask has been used, the estimate of $\delta_g(\mathbf{x})$ is unbiased, but has spatially varying noise, and we only have estimates within the volume covered by the survey. In order to optimally measure the amplitude of clustering, we need to apply weights. If we assume that the galaxy field forms a Poisson sampling of a field with expected power spectrum $\bar{P}(k)$, then the optimal weights to use are

$$w(\mathbf{x}) = \frac{1}{1 + \bar{n}(\mathbf{x})\bar{P}(k)} \, , \tag{25}$$

where $\bar{n}(\mathbf{x})$ is the expected density of galaxies (Feldman *et al.* 1994). The dependence on both $\bar{n}(\mathbf{x})$ and $\bar{P}(k)$ in these weights balances the shot-noise and sample-variance components of the measurement error. For multiple samples of galaxies covering the same volume, but with different expected clustering strengths (each sample is given a subscript i), the optimal weights (Percival *et al.* 2004) to apply are

$$w_i(\mathbf{x}) = \frac{\bar{P}_i(k)}{1 + \sum_i \bar{n}_i(\mathbf{x})\bar{P}_i(k)} \, . \tag{26}$$

These weights provide the same balance between shot-noise and sample variance as Eq. 25, but now also balance this against the clustering strength of each sample. For example, galaxies

with high clustering strength are up-weighted as these contain higher signal-to-noise. These weighting schemes assume that galaxies Poisson sample the underlying matter field, but this is only an approximation. In fact, galaxies live in matter haloes, and haloes do not Poisson sample the mass in the Universe: on large-scales the matter has a distribution with sub-Poisson variance. Thus applying a weighting based on the mass of the haloes within which the galaxies reside can reduce the shot noise in surveys (Seljak *et al.* 2009).

4.3   Measuring the power spectrum

If we only wish to measure the isotropically averaged power spectrum, then it is possible to simply measure this directly from a Fourier transform of the over-density field (Feldman *et al.* 1994). Suppose that we have a galaxy catalogue with density $n_g(\mathbf{x})$, and a random catalogue describing the mask with density $n_r(\mathbf{x})$ containing α times as many objects. Following Feldman *et al.* (1994), we start from the un-normalised over-density field

$$F(\mathbf{x}) = n_g(\mathbf{x}) - n_r(\mathbf{x})/\alpha \,. \tag{27}$$

Taking the Fourier transform of this field, and calculating the power gives

$$\langle|F(\mathbf{k})|^2\rangle = \int \frac{d^3k'}{(2\pi)^3}[P(\mathbf{k}') - P(0)\delta_D(\mathbf{k})]|G(\mathbf{k} - \mathbf{k}')|^2 + (1 + \frac{1}{\alpha})\int d^3x \bar{n}(\mathbf{x}) \,, \tag{28}$$

where $G(\mathbf{k})$ is the Fourier transform of the window function, defined by

$$G(\mathbf{k}) \equiv \int \bar{n}(\mathbf{x})e^{i\mathbf{k}\cdot\mathbf{r}}d^3x \,, \tag{29}$$

and the final term in Eq. 28 gives the shot noise. We see that the effect of the survey mask, which is multiplicative in real-space (think of seeing the Universe through a window only revealing the patch observed), becomes a convolution in Fourier-space. There is a shot noise contribution on all scales, which can be subtracted from the power spectrum estimates, although it still contributes to the error. The fact that we have to estimate the mean density of galaxies from the sample itself means that the $k = 0$ mode is artificially set to zero, equivalent to subtracting a single Dirac delta function from the centre of the un-convolved power. The equivalent correction for correlation function estimates is commonly know as the "Integral constraint"

The comoving power spectrum, as measured from the Data Release 9 (DR9) BOSS data, using the Feldman *et al.* (1994) technique is shown in Fig. 3. The inset shows the ratio of the measured power to a smooth fit, isolating the signature of baryons (see Section 2.3), which is clearly visible (Anderson *et al.* 2012).

We cannot easily measure the anisotropic power spectrum as a function of μ (see Section 1.5) using Fourier methods because the line-of-sight varies across a survey, and does not line-up with a Cartesian grid. Thus, to measure the anisotropic power spectrum, one either needs to manually perform the transform, so a different line-of-sight can be used for each galaxy pair (Yamamoto *et al.* 2006), or decompose into a basis that is itself separable along and across the spatially varying line-of-sight (e.g. Heavens and Taylor 1995). As surveys increase in size and statistical errors reduce, methods such as these will become increasingly important.

4.4   Measuring the correlation function

In order to estimate the correlation function, we can directly make use of the idea of "throwing down sticks" described in Section 1.2. Suppose that the mask is quantified by a random catalogue
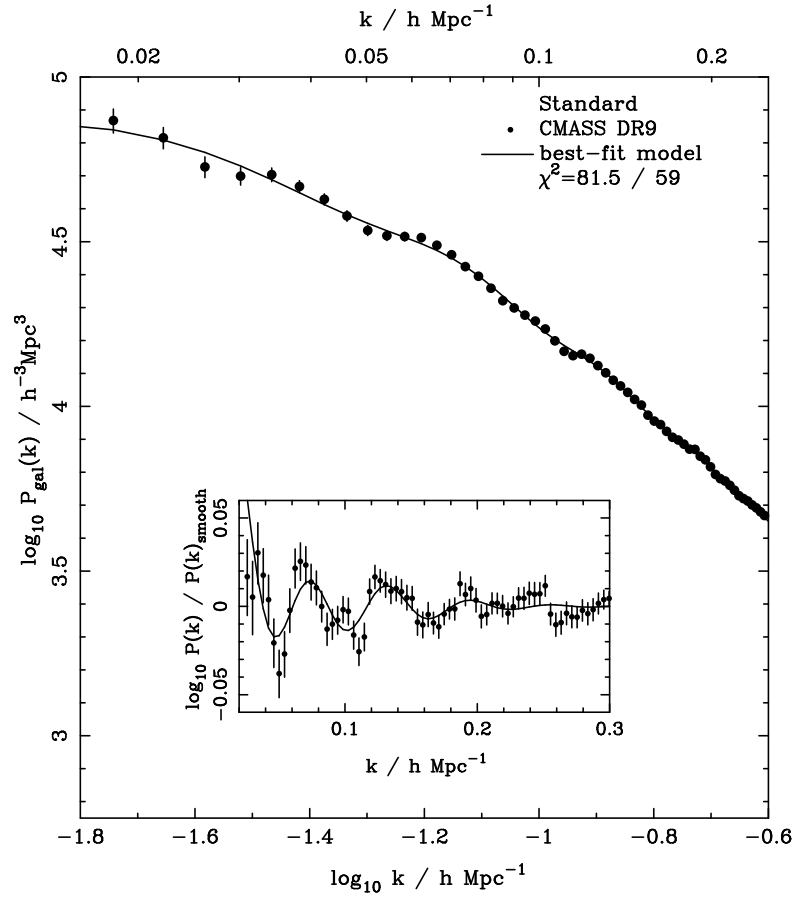
Figure 3: The spherically averaged BOSS DR9 power spectrum for the CMASS galaxy sample (solid circles with 1σ errors), calculated using the method of Feldman *et al.* (1994). The vertical dotted lines show the range of scales fitted ($0.02 < k < 0.3\,\mathrm{h\,Mpc^{-1}}$), and the inset shows the BAO within this k-range, determined by dividing both model and data by the smooth best-fit model. Plot from Anderson *et al.* (2012).

as in Section 4.3, then we can form an estimate of the correlation function $\bar{\xi}$

$$\bar{\xi}(r) = \frac{DD(r)}{RR(r)} - 1 \, , \tag{30}$$

where $DD(r)$ is the number of galaxy-galaxy pairs within a bin with centre r normalised to the maximum possible number of galaxy-galaxy pairs (ie. for n galaxies the maximum number of distinct pairs is $n(n-1)/2$). $RR(r)$ is the normalised number of random-random pairs, and we can similarly define $DR(r)$ as the normalised number of galaxy-random pairs.

This estimate of $\xi(r)$ is biased and we find that

$$\langle 1 + \bar{\xi}(r) \rangle = \frac{1 + \xi(r)}{1 + \xi_\Omega(r)} \, , \tag{31}$$

where $\xi_\Omega(r)$ is the mean of the two-point correlation function over the mask (Landy and Szalay 1993): this corrects for the fact that the true mean density of galaxies $\bar{n}(\mathbf{r})$ is estimated from the sample itself, normalising the total number of pairs. For small samples, the factor $[1 + \xi_\Omega(r)]$, called the "integral constraint", limits the information that can be extracted from $\bar{\xi}(r)$ - in the limit where we only observe pairs of a single separation, $\xi_\Omega \simeq \xi$, and $\bar{\xi}(r)$ contains no information.

Because the galaxy and random catalogues are uncorrelated, $\langle DR(r) \rangle = \langle RR(r) \rangle$, and we can consider a number of alternatives to Eq. 30. In particular

$$\bar{\xi}(r) = \frac{DD(r) - 2DR(r) + RR(r)}{RR(r)} \, , \tag{32}$$

has been shown to have good statistical properties (Landy and Szalay 1993), although Eq. 31 still holds for this estimator (ie. it still "suffers" from the integral constraint). Pair counting methods can be trivially extended to bin pairs in separation and angle to the line-of-sight, giving estimates of the anisotropic correlation function. It is also possible to directly integrate over μ, weighted by a Legendre polynomial to give estimates of the multipoles, or by top-hat windows in μ (called "Wedges"; Kazin $et\ al.$ 2012). These moments of the correlation function provide a mechanism to compress the anisotropic correlation function while still retaining the majority of the available information.

An example correlation function, calculated from the BOSS DR9 CMASS sample (Anderson $et\ al.$ 2012) is given in Fig. 4. The BAO "bump" caused by the physics described in Section 2.3 is clearly visible. On large scales, the correlation function reduces in amplitude (note that $r^2\xi$ is plotted, enhancing the appearance of the large-scale noise), showing that the galaxies are evenly distributed. In fact, conservation of pair number means that the correlation function changes sign on very large scales.

4.5   Reconstructing the linear density

In an evolved density field, pairs of over-densities initially separated by the BAO scale are subject to bulk motions that "smear" the initial pair separations. The matter flows and peculiar velocities act on intermediate scales ($\sim 20\,\mathrm{Mpc\,h^{-1}}$), and therefore suppress small-scale oscillations in the matter power spectrum and smooth the BAO feature in the correlation function (Eisenstein $et\ al.$ 2007b; Crocce and Scoccimarro 2008; Matsubara 2008b; Matsubara 2008a). As galaxies trace the matter density field, the BAO in galaxy surveys are also damped. Eisenstein $et\ al.$ (2007a) suggested that this smoothing can be reversed, in effect using the phase information within the density field to reconstruct linear behaviour. Although not a new idea (e.g. Peebles 1989; Peebles 1990; Nusser and Dekel 1992; Gramann 1993), the dramatic effect on BAO recovery had
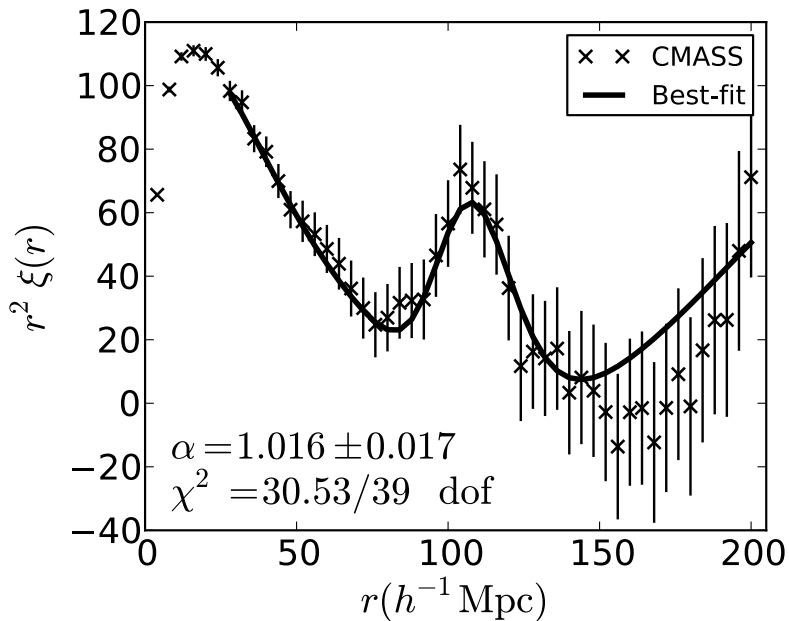
Figure 4: The spherically averaged BOSS DR9 correlation function for the CMASS galaxy sample (solid circles with 1σ errors), calculated using the method of (Landy and Szalay 1993). Plot from Anderson *et al.* (2012).

not been previously realised, and the majority of the benefit was shown to be recovered from a simple reconstruction prescription.

"Reconstruction" has been used to sharpen the BAO feature and improve distance constraints on mock data (Padmanabhan and White 2009; Noh *et al.* 2009; Seo *et al.* 2010; Mehta *et al.* 2011), and was recently applied to the SDSS-II Luminous Red Galaxy (LRG) sample (Padmanabhan *et al.* 2012). The reconstruction was particularly effective in this case, providing a 1.9 per cent distance measurement at $z = 0.35$, decreasing the error by a factor of 1.7 compared with the pre-reconstruction measurement. On the BOSS DR9 CMASS sample, however, reconstruction was not as effective, and did not significantly reduce the error on the BAO scale measurement. Anderson *et al.* (2012) showed, using mock catalogues, that this is expected, and that the effectiveness of reconstruction varies across mocks. The average effect of reconstruction on the BOSS DR9 CMASS mocks is shown in Fig. 5.

4.6   Ly-α forest surveys

Light from distant quasars passes through intervening clouds of gas that absorb ultraviolet light predominantly at the wavelength of the Lyman alpha transition in neutral hydrogen (122 nm). The absorbing clouds are all at lower redshift than the quasar, so absorption lines are on the shorter wavelength side of the quasar emission line. Thus, if we divide the quasar spectrum by the expected continuum for each quasar, we are left with a 1D absorber over-density profile, which can be used to estimate the matter over-density field along the line-of-sight in much the same way that galaxies can be used directly (in fact the link between absorber density and matter density is more complicated than between galaxies and the mass). The great thing about using the Ly-α
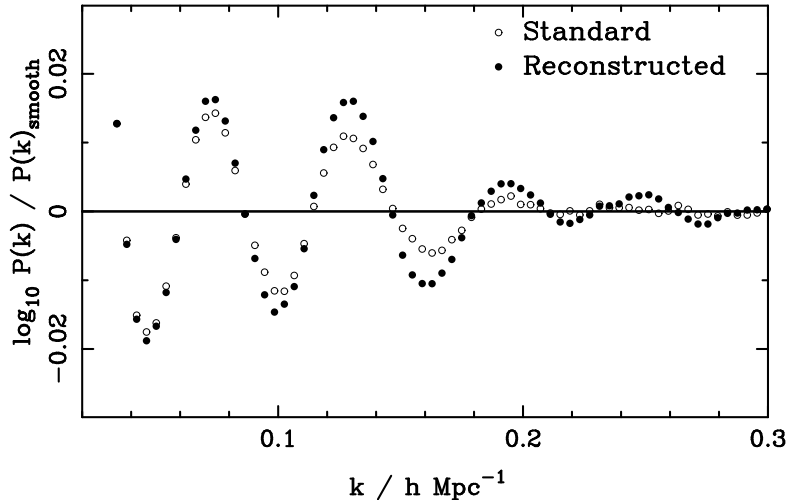
Figure 5: The ratio between recovered power spectrum and smooth fit for the 600 BOSS DR9 CMASS catalogues, before and after applying a simple reconstruction algorithm. We see that, on average, reconstruction acts to improve the BAO signal on small scales. Plot from Anderson *et al.* (2012).

forest is that a single spectrum gives information about multiple structures along the line of sight, and thus this method provides a highly efficient use of telescopes. Using quasars with $z > 2.15$, the BOSS has made BAO measurements using Lyman α forest in quasar spectra, extending BAO measurements into the redshift range $2 < z < 3.5$ (Busca *et al.* 2013; Slosar *et al.* 2013; Kirkby *et al.* 2013).

5 Observational effects

Up to this point, we have been concerned with comoving galaxy clustering, and the information it contains. In fact, a lot of the information from galaxy surveys does not come directly from the comoving power, but from effects that distort the observed signal away from this ideal. We now outline three of these effects, showing how they can be used to retrieve cosmological information.

5.1 Projection and the Alcock-Paczynski effect

The physics described above is encoded into the comoving galaxy power spectrum. However, we do not measure clustering directly in comoving space, but we instead measure galaxy redshifts and angles and infer distances from these. If we use the wrong cosmological model to do this conversion, then the distances we infer will be wrong and the comoving clustering will contain detectable distortions.

In the radial direction, provided that the clustering signal is small compared with the cosmological distortions, we are sensitive to the Hubble parameter through $1/H(z)$. In the angular direction the distortions depend on the angular diameter distance $D_A(z)$. Adjusting the cosmological model to ensure that angular and radial clustering match constrains $H(z)D_A(z)$, and was first proposed as a cosmological test (the AP test) by Alcock and Paczynski (1979). If we

instead consider averaging clustering in 3D over all directions, then, to first order, matching the scale of clustering measurements to the comoving clustering expected is sensitive to

$$D_V(z) = \left[(1+z)^2 D_A^2(z) \frac{cz}{H(z)} \right]^{1/3} . \qquad (33)$$

Although this projection applies to all of the clustering signal, BAO provide the most robust and strongest source for the comparison between observed and expected clustering, providing a distinct feature on sufficiently large scales that it is difficult to alter with non-linear physics. In order to extract this information, we need to parametrize over nuisance broad-band features, extracting just the BAO signal. This is usually achieved by means of a smooth function, commonly a polynomial or spline with a set of free parameters, with sufficient flexibility to match the broad-band shape of all of the cosmological models to be tested, but not the BAO signal. If a fiducial cosmological model is used to convert redshifts to distances, then departures between the expected BAO position, and the observed one are commonly quantified by dilation scales. For an anisotropic fit, we can define two dilation scales, perpendicular and parallel to the line-of-sight

$$\alpha_\perp = \frac{D_A(z) r_d^{\mathrm{fid}}}{D_A^{\mathrm{fid}} r_d} , \quad \alpha_\parallel = \frac{H^{\mathrm{fid}}(z) r_d^{\mathrm{fid}}}{H(z) r_d} , \qquad (34)$$

where r_d sets the comoving BAO scale (see Section 2.3), and a superscript fid denotes that a quantity refers to the fiducial cosmology used to measure the clustering signal. For a single fit to the BAO in an isotropically averaged clustering measurement, the combined dilation scale is

$$\alpha = \frac{D_V(z) r_d^{\mathrm{fid}}}{D_V^{\mathrm{fid}} r_d} . \qquad (35)$$

Estimates of the BAO scale can be made based on either $\xi(r)$ or $P(k)$, but they include the noise from small scales and shot noise differently. Anderson *et al.* (2012) averaged measurements made from both statistics, using mocks to show that this improved the combined error.

A review of current BAO measurements was provided in the introduction of Anderson *et al.* (2012), which described recent experiments (e.g. Beutler *et al.* 2011; Blake *et al.* 2011; Padmanabhan *et al.* 2012), leading to the analyses presented in (Anderson *et al.* 2012). Since then, the DR9 data set has been analysed splitting into measurements along and across the line-of-sight (Anderson *et al.* 2013), and the next release of measurements from BOSS is imminent. In addition, the range of redshifts covered by BAO measurements has increased further, through BOSS analyses using the Lyman-α forest in quasar spectra (Busca *et al.* 2013; Slosar *et al.* 2013; Kirkby *et al.* 2013).

5.2 Redshift-space distortions

The second observational effect that we will consider results from the fact that our estimates of galaxy distances are made from redshifts. These redshifts are caused by both the Hubble expansion and from any additional motion within a comoving frame, called the peculiar velocity. We can write

$$\mathbf{s}(\mathbf{r}) = \mathbf{r} - v_r(r)\frac{\mathbf{r}}{r} , \qquad (36)$$

where $\mathbf{s}$ is the redshift-space (i.e. derived from the redshift) position of a galaxy, $\mathbf{r}$ is the true real-space position of the galaxy away with the observer at the origin, and $v_r(r)$ is the radial component of the peculiar velocity. The distortions in the field that result from the peculiar-velocity dependent shifts are called Redshift-Space Distortions (RSD).
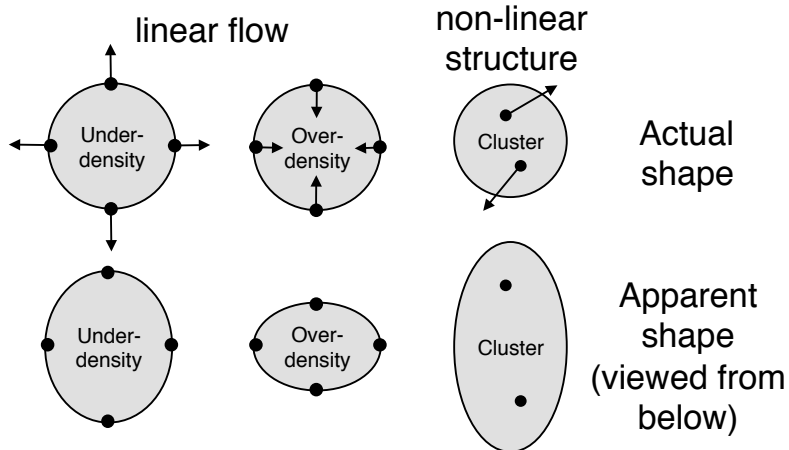
Figure 6: Explanatory diagram showing how real-space structures (top row) look in redshift-space (bottom row).

Locally, galaxies act as test particles in the flow of matter. If galaxies fully sampled the velocity field, the peculiar velocity distribution of galaxies would match that of the mass. We should be aware that galaxies are expected to be at special locations in the density field, potentially giving rise to a small bias in their velocity distribution compared to that of the mass.

As discussed in Section 3.1, structures are continually growing through gravity. On large-scales this growth is the dominant source of RSD. Consider a galaxy on the near-edge of a strong over-density: this galaxy will tend to be falling in to the over-density, away from us, increasing its redshift and moving its apparent position closer to the centre of the over-density. A galaxy at the far-edge of an over-density will appear closer, and we therefore see that clusters will appear "squashed" along the line-of-sight in redshift-space. By a similar argument, under-dense regions appear "stretched" along the line-of-sight. This is shown in Fig. 6.

If we assume that the patch of the Universe from which clustering is measured is sufficiently far away that the line-of-sight is approximately constant across the patch, this effect causes an increase in the measured power that can be easily modelled. Following Kaiser (1987), on linear scales we can derive a change in the power corresponding to

$$P_{gg}^s(k,\mu) = P_{gg}^r(k) + 2\mu^2 P_{g\theta}^r(k) + \mu^4 P_{\theta\theta}^r(k) \,, \tag{37}$$

where $\theta = \nabla \cdot \mathbf{v}$ is the divergence of the peculiar velocity field, a superscript s denotes that a quantity is measured in redshift-space and r in real-space, and a subscript g denotes that a quantity refers to the galaxy field. Furthermore, in the linear regime, we can write $\theta = -f\delta_m$, where m refers to the matter field, and

$$f \equiv \frac{d\ln G}{d\ln a} \,, \tag{38}$$

is the logarithmic derivative of the linear growth rate. Assuming a linear bias, we can write $\delta_g^r = b\delta_m^r$, and we see that the amplitude of the anisotropic power spectrum given in Eq. (37) depends on $b\sigma_8$ and $f\sigma_8$, where σ_8 is the standard deviation of the distribution of over-densities when averaged over spheres of radius $8\,\mathrm{Mpc\,h^{-1}}$. If we spherically average the power spectrum,

19

equivalent to integrating over $0 < \mu < 1$, we find that

$$P_{gg}^s = P_{mm}^r \left[b^2 + \frac{2}{3}bf + \frac{1}{5}f^2 \right] . \tag{39}$$

On small-scales, there is a second RSD effect caused by galaxy motion within collapsed objects with deep potential wells. The random velocities attained by such galaxies smear the collapsed object along the line of sight in redshift space, leading to the existence of linear structures pointing towards the observer in redshift-space. This is shown in Fig. 6. These apparent structures are known as "Fingers-of-God" (FoG) and reduce information on small scales. If the pairwise velocity dispersion within a collapsed object has an exponential distribution (superposition of Gaussians), then we get a multiplicative damping term for the power spectrum of the form

$$F_{\text{fog}}(k, \mu) = \left(1 + \frac{k^2 \mu^2 \sigma_p^2}{2} \right)^{-1} , \tag{40}$$

where $\sigma_p \sim 400 \, \text{kms}^{-1}$ (Hawkins *et al.* 2003). It is common to multiply $P_{gg}^s(k, \mu)$ from Eq. (37) by $F_{\text{fog}}(k, \mu)$ to provide a combined model for the anisotropic power spectrum. However this model is not guaranteed to work in the quasi-linear regime, although the damping term can model some of the quasi-linear signal if σ_p is treated as a free parameter (Percival and White 2009).

An alternative to modelling the FoG is to try to correct data by using phase information to "collapse clusters" along the line of sight (e.g. Tegmark *et al.* 2004). This method has similarities with "reconstruction" used to recover BAO information. For the SDSS-II Luminous Red Galaxy sample, Reid *et al.* (2010) used an anisotropic friends-of-friends group finder, normalised using numerical simulations (Reid *et al.* 2009) to locate clusters and move the galaxies to the average redshift, removing much of the FoG signal and reducing the modelling burden.

Standard measurements of the RSD signal are intrinsically limited by the number of radial modes present, which provide the sample variance limit. McDonald and Seljak (2009) showed that, with two samples of galaxies covering the same region, it is possible to measure ratios of power spectra independent of cosmic variance - provided that the two samples both have different linear deterministic biases. Taking into account the anisotropic nature of their redshift-space power spectrum, shot-noise limited measurements of f/b_i and b_i/b_j (where i, j refer to the galaxy samples) would be possible. These combine to give measurements of $f\sigma_8$ that are limited by the total number of modes within a survey, rather than just those in the radial direction - potentially a strong source of further information.

The picture for RSD measurements presented in this section relies on a number of assumptions, particularly the combination of linear theory with a simple damping model, and the assumption that we are only interested in pairs of galaxies for which the line-of-sights are approximately parallel. These assumptions have been tested and shown to be adequate for current RSD growth rate measurements (Samushia *et al.* 2012). Many RSD-based measurements of the growth rate have been made from a number of spectroscopic surveys, with a recent compilation provided in Reid *et al.* 2012.

5.3 Joint AP and RSD measurements

The primary problem with making RSD and AP measurements of the full (not just BAO) clustering signal is disentangling both effects (Ballinger *et al.* 1996), although Samushia *et al.* (2012) showed how future surveys ameliorate this problem. For current surveys, this separation can only be achieved on large-scales, where RSD can be modelled with perturbation theory, leading to joint RSD and AP measurements (e.g. Reid *et al.* 2012). The power of the large-scale AP test

was shown in Samushia *et al.* (2013), who demonstrated that using the joint $H(z)$ and $D_A(z)$ AP measurements of Reid *et al.* (2012) led to a fortuitous degeneracy breaking compared with using the isotropic BAO measurements of Anderson *et al.* (2012). This led to a factor of five improvement on measuring the Dark Energy equation-of-state $w(z = 0.57)$, which is particularly impressive given that the same data were used to make both measurements.

5.4   Primordial non-Gaussianity

As discussed in Section 2, determining the amount of primordial non-Gaussianity in the matter over-density field provides a key way of distinguishing between inflationary models. Observations of the large-scale clustering of galaxies have the potential to measure this, as we will now demonstrate. One of the simplest way to parameterise non-Gaussianity is to assume that the potential has a local quadratic term

$$\Phi = \phi + f_{NL} \left(\phi^2 - \langle \phi^2 \rangle \right) . \tag{41}$$

Although many other forms of non-Gaussianity are possible, any detection of non-Gaussianity would be interesting, and it is therefore instructive to consider how this simple model can be constrained by galaxy clustering measurements (Dalal *et al.* 2008).

We can see this by reconsidering the peak-background split model - in Section 3.4, we saw that halo formation is much easier with additional long-wavelength fluctuations. If we decompose the potential in Eq. (41) into long (ϕ_l) and short (ϕ_s) wavelength components, we find that

$$\Phi = \phi_l + f_{NL}\phi_l^2 + (1 + 2f_{NL}\phi_l)\phi_s + f_{NL}\phi_s^2 + \text{cnst} . \tag{42}$$

The $f_{NL}\phi_l^2$ term is small, but we see that there is an extra term $2f_{NL}\phi_l\phi_s$, which is of importance for the large-scale bias. To see how this enters into the peak-background split model, note that the link between over-density and potential can be written $\delta_l(k) = \alpha(k)\phi(k)$, where

$$\alpha(k) = \frac{2c^2k^2T(k)G(z)}{3\Omega_M H_0^2} . \tag{43}$$

Now, one factor of α gets absorbed into converting one of the potentials in the extra term to an over-density, but we are left with a critical density that is modulated not just by the Gaussian long-wavelength fluctuation, but by

$$\delta_l + 2f_{NL}\phi_l = \delta_l \left(1 + \frac{2f_{NL}}{\alpha(k)} \right) . \tag{44}$$

This extra term propagates into the change in number density of haloes and the bias as determined by the peak-background split model

$$n \quad \rightarrow \quad n - \left(1 + \frac{2f_{NL}}{\alpha(k)} \right) \frac{dn}{d\delta_c}\delta_l , \tag{45}$$

$$b \quad = \quad 1 - \left(1 + \frac{2f_{NL}}{\alpha(k)} \right) \frac{d\ln n}{d\delta_c} . \tag{46}$$

Because of the k^2 term in $\alpha(k)$, the bias diverges to large-scales, giving a detectable signature with amplitude dependent on f_{NL}.

Unfortunately, the large-scale clustering signal is one of the most difficult to measure, not just because large volumes are required to reduce sample variance. In fact, observational systematics can strongly affect the clustering on large-scales. For the SDSS, variations in stellar density and seeing for imaging data can lead to target density fluctuations giving rise to
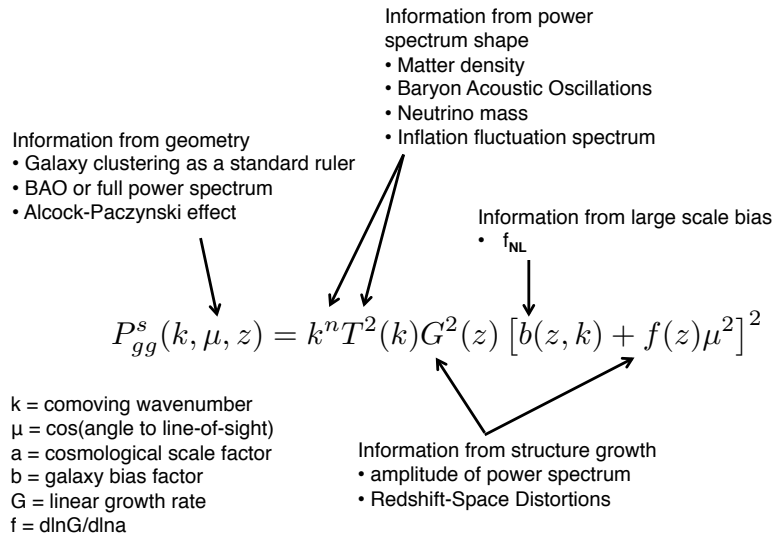
Figure 7: Summary of the physics encoded in the observed large-scale galaxy clustering signal, as described by the linear power spectrum.

large-scale power in spectroscopic galaxy samples that is degenerate with the f_{NL} signature (Ross *et al.* 2011; Ross *et al.* 2012). Current galaxy survey measurements of local f_{NL} are consistent with $f_{NL} = 0$, with contraints from galaxy surveys giving measurements of $f_{NL} \pm 21$ at 1σ (Giannantonio *et al.* 2013), which should be compared with those from the CMB, which are of order ± 5 (Planck Collaboration *et al.* 2013*a*).

5.5   Summary

A summary of the physics encoded within the linear galaxy power spectrum is presented in Fig. 7. This provides a simple model for the power spectrum, showing the measurements that can be made from each component.

6   Making cosmological-model inferences

Modern observational cosmology relies on combining multiple observations to make inferences about the correct cosmological model. It uses Bayes theorem to do this. Suppose we have a hypothesis to be tested H, a set of things assumed to be true I (for example the model of the observations), and a set of data d, then Bayes theorem gives that

$$p(H|d, I) = \frac{p(d|H, I)p(H|I)}{p(d|I)}, \tag{47}$$

where $L(H) \equiv p(d|H, I)$ is the sampling distribution of data, often called the Likelihood, $p(H|I)$ is the prior, $p(d|I)$ the normalisation, and $p(H|d, I)$ the posterior probability.

The hypothesis to be tested is often a vector of parameters θ, which can be split into interesting ϕ (e.g. the dark energy equation of state $w(z)$), and uninteresting ψ (e.g. the parameters of

the smooth fit to the broad-band power when extracting the BAO signal) parameters. Parameter inference is performed as

$$p(\theta|d, I) \propto \int L(\phi, \psi)p(\phi, \psi|I)d\psi \,, \qquad (48)$$

in order to marginalise over the nuisance parameters, while retaining information about the interesting parameters. Often we wish to know the probability distribution for each parameter in turn having marginalised over all others.

The primary concern when making parameter inferences is keeping a handle on the physics that is being used, and allowing for all of the potential sources of systematic error. When multiple data sets are combined it becomes difficult to follow systematics through the procedure, or to understand which parts of the constraints are coming from which data set. In addition, a prior is required for the hypothesis, whose impact can sometime be large, such that constraints come from this, rather than the data.

6.1 Exploring parameter space

Often, the list of parameters is long, and thus multi-parameter likelihood calculations would be computationally expensive using grid-based techniques. Consequently, fast methods to explore parameter spaces are popular, particularly the Markov-Chain Monte-Carlo (MCMC) technique, which is commonly used for such analyses. While there is publicly available code to calculate cosmological model constraints (Lewis and Bridle 2002), the basic method is extremely simple and relatively straightforward to code.

The MCMC method provides a mechanism to generate a random sequence of parameter values whose distribution matches the posterior probability distribution. These sequences of parameter, or "chains" are commonly generated by an algorithm called the Metropolis algorithm (Metropolis *et al.* 1953): given a chain at position $\mathbf{x}$, a candidate point $\mathbf{x_p}$ is chosen at random from a proposal distribution $f(\mathbf{x_p}|\mathbf{x})$ - usually by means of a random number generator tuned to this proposal distribution. This point is always accepted, and the chain moves to point $\mathbf{x_p}$, if the new position has a higher likelihood. If the new position $\mathbf{x_p}$ is less likely than $\mathbf{x}$, then we must draw another random variable, this time with uniform density between 0 and 1. $\mathbf{x_p}$ is accepted, and the chain moves to point $\mathbf{x_p}$if the random variable is less than the ratio of the likelihood of $\mathbf{x_p}$ and the likelihood of $\mathbf{x}$. Otherwise the chain "stays" at $\mathbf{x}$, giving this point extra weight within the sequence. In the limit of an infinite number of steps, the chains will reach a converged distribution where the distribution of chain links are representative of the likelihood hyper-surface, given any symmetric proposal distribution $f(\mathbf{x_p}|\mathbf{x}) = f(\mathbf{x}|\mathbf{x_p})$ (see, for example, Roberts 1996).

It is common to implement dynamic optimisation of the sampling of the likelihood surface (see other articles in the same volume as Roberts 1996 for examples), performed in a period of burn-in at the start of the process. One thorny issue is convergence – how do we know when we have sufficiently long chains that we have adequately sampled the posterior probability. A number of tests are available (Gelman and Rubin 1992; Verde *et al.* 2003), although it's common to also test that the same result is obtained from different chains started at widely separated locations in parameter space.

6.2 Model selection

A lot of the big questions to be faced by future experiments can be reduced to understanding whether a simple model is correct, or whether additional parameters (and/or physics) are needed. For example, a lot of future experiments are being set up to test whether the simple ΛCDM

23

model is correct. A model with more parameters will always fit the data better than a model with less parameters (provided it replicates the original model), while removing parameters may or may not have a large impact on the fit. The interesting question is whether the improvement allowed by having an extra free parameter is sufficient to show that a parameter is needed? Bayes theorem, Eq. (47), can test the balance between quality of fit and the predictive ability, potentially providing an answer to these problems.

The Bayesian evidence is defined as the average of the Likelihood under the prior, given by $p(d|I)$ in Eq. (47). Splitting into model and parameters,

$$p(d|I) = \int_{\theta} p(d|\theta, M) p(\theta|M) d\theta \,. \tag{49}$$

The Bayes factor is defined as the ratio of the evidence for two models

$$B_{01} = \frac{p(d|I_0)}{p(d|I_1)} \,. \tag{50}$$

The strength of the evidence that the Bayes factor gives is often quantified by the Jeffries scale, which requires $B_{01} > 2.5$ to give moderate evidence for an additional parameter, and $B_{01} > 5.0$ for strong evidence.

One problem with this approach is that the results depends on the prior that is placed on the new parameter. For a wide prior covering regions in parameter space that are unlikely, the average likelihood and Bayes factor are reduced. A tight prior around the best-fit position will lead to an increase in the Bayes factor. Because of this, many variations on this test for new parameters have been proposed (e.g. review by Trotta 2008).

7 Future surveys

A number of galaxy and Ly-α surveys are planned for the future, in order to build up a picture of the distance-redshift relation over a wide range of redshifts.

7.1 The next 5 years

The Sloan telescope will start to perform a spectroscopic galaxy survey in 2014, called the extended Baryon Oscillation Spectroscopic Survey (**eBOSS**: http://www.sdss3.org/future/). This is the cosmological survey within SDSS-IV, a six-year program using existing hardware and an updated redshift measurement software pipeline. eBOSS will provide distance measurements with BAO in the redshift range $0.6 < z < 2.5$, approximately equivalent to a 1% distance measurement at $z = 0.8$, two 2% measurements at higher redshifts $z \sim 0.9$ and $z \sim 1.5$ and a 1.5% measurement at $z = 2.5$ from clustering within the Ly-α forest observed in the spectra from distant quasars. These measurements will be complemented with RSD measurements.

The Dark Energy Survey (**DES**: www.darkenergysurvey.com) is using a new 520-megapixel camera on the NOAO CTIO 4-meter Blanco telescope to perform a $5000 \, \mathrm{deg}^2$ multi-colour (grizY) imaging survey of the southern hemisphere. When combined with VISTA data, this will provide photometric redshifts for 180,000,000 galaxies out to $z = 1.5$. The project is designed so that this catalogue can be used to measure the equation of state of dark energy through the combination of measurements from cluster number densities, weak lensing, supernovae and galaxy clustering. Survey operations have recently started (Autumn 2013), with a 5-year baseline duration. Because only photometric redshifts are available, only angular BAO will be measurable, and when the

data is combined we expect DES to provide a $\sim 2\%$ measurement of the BAO distance scale at $z = 1$.

Over 3 years, the Hobby-Eberly Telescope Dark Energy Experiment (**HETDEX**) will take spectra and measure redshifts for 800,000 Ly-α emitting galaxies at $1.9 < z < 3.5$ over $420\,\mathrm{deg}^2$. Predictions for this survey are provided in Greig *et al.* (2013), which suggest that a 1.2% distance measurement at $z = 2.7$ is possible.

Two collaborations, Physics of the Accelerating Universe (**PAU**) and Javalambre Physics of the Accelerating Universe Astrophysical Survey (**J-PAS**), are building new imaging cameras with the aim of performing narrow-band imaging surveys, where excellent photometric redshift can be obtained for of order 2-10,000,000 galaxies. PAU will be based on the William Herschel Telescope (WHT), whereas J-PAS will use a new dedicated 2.5m telescope in the South of Spain. Both surveys envisage starting in 2014, and running for ~ 5 years. Even using narrow-band filters, the degradation due to having photometric redshifts means that these surveys will be superseded by the next generation of spectroscopic redshift surveys.

7.2 5-20 years time

The next step for ground-based surveys is to place and utilise a new multi-object spectrograph, capable of obtaining many thousands of spectra simultaneously, on a 4m-class telescope. One project, called Dark-Energy Spectroscopic Instrument (**DESI**), will fit the Mayall telescope with a new ~ 5000-fibre spectrograph covering a 2–$3\,\mathrm{deg}$ diameter field. DESI is the most ambitious extra-galactic ground-based survey proposed to date, given the fibre number, field of view and fibre reconfiguration time (Schlegel *et al.* 2011). Survey operations would be expected to commence in 2018. Other multi-object spectrographs being designed for 4m telescopes include WEAVE (Dalton *et al.* 2012) and 4MOST (de Jong *et al.* 2012).

The Subaru telescope Prime Focus Spectrograph (**PFS**) is a new spectrograph due to have first light in 2017. It will have 2400 fibres, covering a $1.3\,\mathrm{deg}$ diameter field of view (Takada *et al.* 2012). The current cosmology survey design envisages a survey over $1500\,\mathrm{deg}^2$, yielding 3,000,000 galaxies over $0.6 < z < 2.4$.

Looking beyond these ground-based surveys, the ESA **Euclid** mission, with a nominal launch date of 2019, will revolutionise observational cosmology by conducting imaging and spectroscopic surveys that are approximately two orders of magnitude better than those currently available (Laureijs *et al.* 2011).

7.3 Fisher methods

It is common to make predictions for future surveys, in order to compare them to each other and optimise them individually, using Fisher methods. From Section 6, we have the Likelihood $L(H)$. Then the Fisher matrix is defined as

$$F_{ij} \equiv \left\langle \frac{\partial^2 \mathcal{L}}{\partial \theta_i \partial \theta_j} \right\rangle , \qquad (51)$$

where $\mathcal{L} \equiv -\ln L$. For a multi-variate Gaussian distribution,

$$F_{ij} = \frac{1}{2} \left[C^{-1} \frac{\partial C}{\partial \theta_i} C^{-1} \frac{\partial C}{\partial \theta_j} \right] + \frac{\partial \mu^T}{\partial \theta_i} C^{-1} \frac{\partial \mu^T}{\partial \theta_j} , \qquad (52)$$

where C is the covariance matrix, and μ the model for the parameters being tested (e.g. power spectrum band-powers). The Cramer-Rao inequality shows that the diagonal elements of the

Fisher matrix give the best model error we can hope to achieve

$$\Delta\theta_i \geq (F_{ii})^{-1/2} . \tag{53}$$

For a sample with constant number density within a volume V, the error on the average power spectrum within a k-volume V_k (e.g. Feldman *et al.* 1994) is

$$\langle P(\mathbf{k})P(\mathbf{k}')\rangle = \frac{1}{VV_k} \left[P(k)\delta_D(\mathbf{k}-\mathbf{k}') + 1/\bar{n}\right]^2 . \tag{54}$$

For a sample with varying density over the region surveyed, we can define an effective volume

$$V_{eff} \equiv \int \left[\frac{\bar{n}(\mathbf{r})P(k)}{1 + \bar{n}(\mathbf{r})P(k)} \right]^2 dr^3 . \tag{55}$$

If the survey is limited by the total number of redshifts that can be obtained, then this has a maximum where $\bar{n}P = 1$. For future surveys we will be limited by the sky area we can observe, the field-of-view of the telescope, or the redshift range we can test with a given spectrograph, so we often have $\bar{n}P \neq 1$. Based on the effective volume,

$$\langle P(\mathbf{k})^2 \rangle = 2\frac{P(k)^2}{V_{eff}V_k} . \tag{56}$$

This gives a Fisher matrix that can be written, if we now integrate over many small shells V_k (Tegmark 1997),

$$F_{ij} = \frac{1}{2}\int \frac{d^3k}{(2\pi)^3} \left(\frac{\partial \ln P}{\partial \theta_i}\right)\left(\frac{\partial \ln P}{\partial \theta_j}\right) V_{eff}(k) . \tag{57}$$

This is the starting point for designing and optimising future surveys. Code that uses these ideas and isolates the BAO signal is provided by Seo and Eisenstein (2007), while code for RSD measurements is given by White *et al.* (2009). Using these codes, we can predict measurement errors on the measured distance scale, or on $f\sigma_8$. Starting either from these measurements or Eq. 57, we can create Fisher matrices spanning the parameters of complete cosmological models.

In order to provide a simple statistic with which to compare experiments, The Dark Energy Task Force (DETF; Albrecht *et al.* 2006) parametrized the equation of state $w(z)$ of dark energy using two parameters w_0 and w_a:

$$w(z) = w_0 + \frac{z}{1+z}w_a . \tag{58}$$

They then defined their Figure-of-Merit (FoM) to be proportional to the inverse area of the error ellipse in the w_0–w_a plane

$$FoM_{\mathrm{DETF}} = [\det C(w_o, w_a)]^{-1/2} , \tag{59}$$

where $C(w_o, w_a)$ is the covariance matrix after marginalising over all of the other cosmological parameters. A larger FoM_{DETF} is desired as it corresponds to a smaller error ellipse. Note that FoM_{DETF} only cares about two parameters: an experiment that measures $w(z)$ very accurately but only over a narrow redshift range will score well. As the true dark energy equation-of-state is unknown, so FoM_{DETF} is not necessarily the best statistic with which to compare the discovery potential of multiple projects. Other options that attempt to alleviate these problems are available (e.g. Albrecht *et al.* 2009).
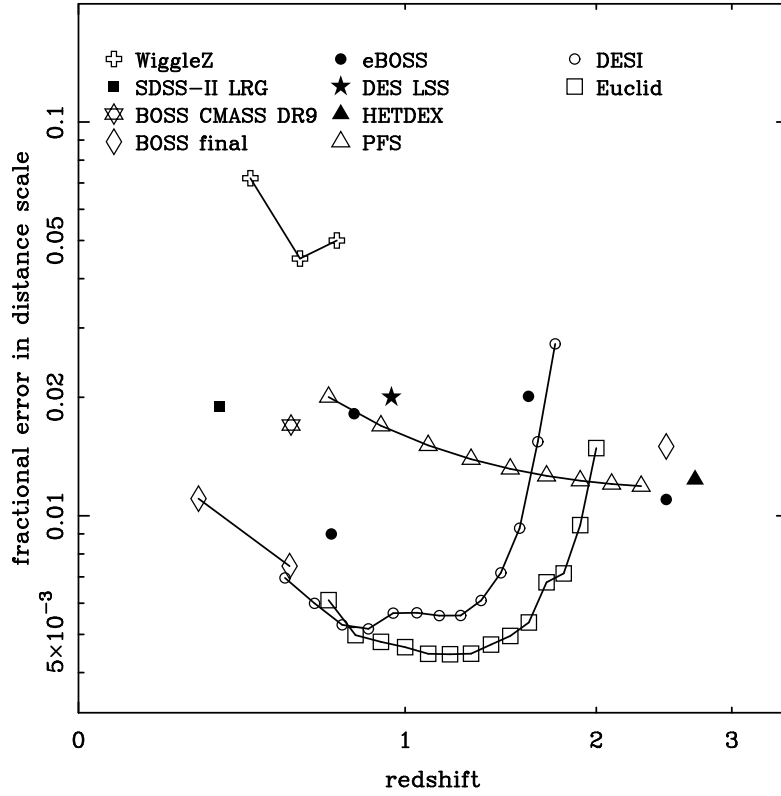
Figure 8: Predictions for BAO measurements from the surveys introduced in Sections 7.1 & 7.2, calculated using the code of Seo and Eisenstein (2007).

7.4 Predictions for future surveys

Predicted BAO measurements for the surveys introduced in Sections 7.1 & 7.2, are presented in Fig. 8. The final BOSS galaxy survey is predicted to provide multiple sub-percent BAO measurements out to redshifts of $z \sim 0.6$. Surveys that are starting now will provide 1–2% measurements over a wider redshift range, including percent level measurements from the Ly-α forest. The next generation of surveys including DESI and Euclid will provide multiple sub-percent level measurements within redshift bins of width $\Delta z = 0.1$ over the full redshift range $0.6 < z < 2.0$.

In order to realise the power of future surveys, we will need systematic errors that are significantly below the level of the statistical errors shown in Fig. 8. To ensure this, all aspects of the analysis will need to be evaluated for potential errors, including the likelihood calculation, and model to be fitted to the data. Provided this is achieved then the future surveys will provide a stunning new insight into the evolution of the Universe and the forces driving it.

References

Albrecht, A., Amendola, L., Bernstein, G., Clowe, D., Eisenstein, D., Guzzo, L., Hirata, C., Huterer, D., Kirshner, R., Kolb, E., and Nichol, R. (2009, January). Findings of the Joint Dark Energy Mission Figure of Merit Science Working Group. *ArXiv e-prints*.

Albrecht, A., Bernstein, G., Cahn, R., Freedman, W. L., Hewitt, J., Hu, W., Huth, J., Kamionkowski, M., Kolb, E. W., Knox, L., Mather, J. C., Staggs, S., and Suntzeff, N. B. (2006, September). Report of the Dark Energy Task Force. *ArXiv Astrophysics e-prints*.

Alcock, C. and Paczynski, B. (1979, October). An evolution free test for non-zero cosmological constant. Nature , **281**, 358.

Anderson, L., Aubourg, E., Bailey, S., Beutler, F., Bolton, A. S., Brinkmann, J., Brownstein, J. R., Chuang, C.-H., Cuesta, A. J., Dawson, K. S., Eisenstein, D. J., Honscheid, K., Kazin, E. A., Kirkby, D., Manera, M., McBride, C. K., Mena, O., Nichol, R. C., Olmstead, M. D., Padmanabhan, N., Palanque-Delabrouille, N., Percival, W. J., Prada, F., Ross, A. J., Ross, N. P., Sanchez, A. G., Samushia, L., Schlegel, D. J., Schneider, D. P., Seo, H.-J., Strauss, M. A., Thomas, D., Tinker, J. L., Tojeiro, R., Verde, L., Weinberg, D. H., Xu, X., and Yeche, C. (2013, March). The clustering of galaxies in the SDSS-III Baryon Oscillation Spectroscopic Survey: Measuring D_A and H at z=0.57 from the Baryon Acoustic Peak in the Data Release 9 Spectroscopic Galaxy Sample. *ArXiv e-prints*.

Anderson, L., Aubourg, E., Bailey, S., Bizyaev, D., Blanton, M., Bolton, A. S., Brinkmann, J., Brownstein, J. R., Burden, A., Cuesta, A. J., da Costa, L. A. N., Dawson, K. S., de Putter, R., Eisenstein, D. J., Gunn, J. E., Guo, H., Hamilton, J.-C., Harding, P., Ho, S., Honscheid, K., Kazin, E., Kirkby, D., Kneib, J.-P., Labatie, A., Loomis, C., Lupton, R. H., Malanushenko, E., Malanushenko, V., Mandelbaum, R., Manera, M., Maraston, C., McBride, C. K., Mehta, K. T., Mena, O., Montesano, F., Muna, D., Nichol, R. C., Nuza,

S. E., Olmstead, M. D., Oravetz, D., Padmanabhan, N., Palanque-Delabrouille, N., Pan, K., Parejko, J., Pâris, I., Percival, W. J., Petitjean, P., Prada, F., Reid, B., Roe, N. A., Ross, A. J., Ross, N. P., Samushia, L., Sánchez, A. G., Schlegel, D. J., Schneider, D. P., Scóccola, C. G., Seo, H.-J., Sheldon, E. S., Simmons, A., Skibba, R. A., Strauss, M. A., Swanson, M. E. C., Thomas, D., Tinker, J. L., Tojeiro, R., Magaña, M. V., Verde, L., Wagner, C., Wake, D. A., Weaver, B. A., Weinberg, D. H., White, M., Xu, X., Yèche, C., Zehavi, I., and Zhao, G.-B. (2012, December). The clustering of galaxies in the SDSS-III Baryon Oscillation Spectroscopic Survey: baryon acoustic oscillations in the Data Release 9 spectroscopic galaxy sample. Mon. Not. R. Astr. Soc. , **427**, 3435–3467.

Ballinger, W. E., Peacock, J. A., and Heavens, A. F. (1996, October). Measuring the cosmological constant with redshift surveys. Mon. Not. R. Astr. Soc. , **282**, 877.

Bardeen, J. M., Bond, J. R., Kaiser, N., and Szalay, A. S. (1986, May). The statistics of peaks of Gaussian random fields. Astrophys. J. , **304**, 15–61.

Bashinsky, S. and Bertschinger, E. (2001, August). Position-Space Description of the Cosmic Microwave Background and Its Temperature Correlation Function. *Physical Review Letters*, **87**(8), 081301.

Bashinsky, S. and Bertschinger, E. (2002, June). Dynamics of cosmological perturbations in position space. Phys. Rev. D , **65**(12), 123008.

Beutler, F., Blake, C., Colless, M., Jones, D. H., Staveley-Smith, L., Campbell, L., Parker, Q., Saunders, W., and Watson, F. (2011, October). The 6dF Galaxy Survey: baryon acoustic oscillations and the local Hubble constant. Mon. Not. R. Astr. Soc. , **416**, 3017–3032.

Birkhoff, G. D. and Langer, R. E. (1923). *Relativity and modern physics.*

Blake, C., Kazin, E. A., Beutler, F., Davis, T. M., Parkinson, D., Brough, S., Colless, M., Contreras, C., Couch, W., Croom, S., Croton, D., Drinkwater, M. J., Forster, K., Gilbank, D., Gladders, M., Glazebrook, K., Jelliffe, B., Jurek, R. J., Li, I.-H., Madore, B., Martin, D. C., Pimbblet, K., Poole, G. B., Pracy, M., Sharp, R., Wisnioski, E., Woods, D., Wyder, T. K., and Yee, H. K. C. (2011, December). The WiggleZ Dark Energy Survey: mapping the distance-redshift relation with baryon acoustic oscillations. Mon. Not. R. Astr. Soc. , **418**, 1707–1724.

Busca, N. G., Delubac, T., Rich, J., Bailey, S., Font-Ribera, A., Kirkby, D., Le Goff, J.-M., Pieri, M. M., Slosar, A., Aubourg, É., Bautista, J. E., Bizyaev, D., Blomqvist, M., Bolton, A. S., Bovy, J., Brewington, H., Borde, A., Brinkmann, J., Carithers, B., Croft, R. A. C., Dawson, K. S., Ebelke, G., Eisenstein, D. J., Hamilton, J.-C., Ho, S., Hogg, D. W., Honscheid, K., Lee, K.-G., Lundgren, B., Malanushenko, E., Malanushenko, V., Margala, D., Maraston, C., Mehta, K., Miralda-Escudé, J., Myers, A. D., Nichol, R. C., Noterdaeme, P., Olmstead, M. D., Oravetz, D., Palanque-Delabrouille, N., Pan, K., Pâris, I., Percival, W. J., Petitjean, P., Roe, N. A., Rollinde, E., Ross, N. P., Rossi, G., Schlegel, D. J., Schneider, D. P., Shelden, A., Sheldon, E. S., Simmons, A., Snedden, S., Tinker, J. L., Viel, M., Weaver, B. A., Weinberg, D. H., White, M., Yèche, C., and York, D. G. (2013, April). Baryon acoustic oscillations in the Lyα forest of BOSS quasars. Astr. & Astrophys. , **552**, A96.

Byrnes, C. T. and Choi, K.-Y. (2010). Review of Local Non-Gaussianity from Multifield Inflation. *Advances in Astronomy*, **2010**.

Cole, S. (2011, September). Maximum likelihood random galaxy catalogues and luminosity function estimation. Mon. Not. R. Astr. Soc. , **416**, 739–746.

Cole, S. and Kaiser, N. (1989, April). Biased clustering in the cold dark matter cosmogony. Mon. Not. R. Astr. Soc. , **237**, 1127–1146.

Colless, M., Peterson, B. A., Jackson, C., Peacock, J. A., Cole, S., Norberg, P., Baldry, I. K., Baugh, C. M., Bland-Hawthorn, J., Bridges, T., Cannon, R., Collins, C., Couch, W., Cross, N., Dalton, G., De Propris, R., Driver, S. P., Efstathiou, G., Ellis, R. S., Frenk, C. S., Glazebrook, K., Lahav, O., Lewis, I., Lumsden, S., Maddox, S., Madgwick, D., Sutherland, W., and Taylor, K. (2003, June). The 2dF Galaxy Redshift Survey: Final Data Release. *ArXiv Astrophysics e-prints*.

Cooray, A. and Sheth, R. (2002, December). Halo models of large scale structure. Phys. Rep. , **372**, 1–129.

Crocce, M. and Scoccimarro, R. (2008, January). Nonlinear evolution of baryon acoustic oscillations. Phys. Rev. D , **77**(2), 023533.

Dalal, N., Doré, O., Huterer, D., and Shirokov, A. (2008, June). Imprints of primordial non-Gaussianities on large-scale structure: Scale-dependent bias and abundance of virialized objects. Phys. Rev. D , **77**(12), 123514.

Dalton, G., Trager, S. C., Abrams, D. C., Carter, D., Bonifacio, P., Aguerri, J. A. L., MacIntosh, M., Evans, C., Lewis, I., Navarro, R., Agocs, T., Dee, K., Rousset, S., Tosh, I., Middleton, K., Pragt, J., Terrett, D., Brock, M., Benn, C., Verheijen, M., Cano Infantes, D., Bevil, C., Steele, I., Mottram, C., Bates, S., Gribbin, F. J., Rey, J., Rodriguez, L. F., Delgado, J. M., Guinouard, I., Walton, N., Irwin, M. J., Jagourel, P., Stuik, R., Gerlofsma, G., Roelfsma, R., Skillen, I., Ridings, A., Balcells, M., Daban, J.-B., Gouvret, C., Venema, L., and Girard, P. (2012, September). WEAVE: the next generation wide-field spectroscopy facility for the William Herschel Telescope. In *Society of Photo-Optical Instrumentation Engineers (SPIE) Conference Series*, Volume 8446, Society of Photo-Optical Instrumentation Engineers (SPIE) Conference Series.

Dawson, K. S., Schlegel, D. J., Ahn, C. P., Anderson, S. F., Aubourg, É., Bailey, S., Barkhouser, R. H., Bautista, J. E., Beifiori, A., Berlind, A. A., Bhardwaj, V., Bizyaev, D., Blake, C. H., Blanton, M. R., Blomqvist, M., Bolton, A. S., Borde, A., Bovy, J., Brandt, W. N., Brewington, H., Brinkmann, J., Brown, P. J., Brownstein, J. R., Bundy, K., Busca, N. G., Carithers, W., Carnero, A. R., Carr, M. A., Chen, Y., Comparat, J., Connolly, N., Cope, F., Croft, R. A. C., Cuesta, A. J., da Costa, L. N., Davenport, J. R. A., Delubac, T., de Putter, R., Dhital, S., Ealet, A., Ebelke, G. L., Eisenstein, D. J., Escoffier, S., Fan, X., Filiz Ak, N., Finley, H., Font-Ribera, A., Génova-Santos, R., Gunn, J. E., Guo, H., Haggard, D., Hall, P. B., Hamilton, J.-C., Harris, B., Harris, D. W., Ho, S., Hogg, D. W., Holder, D., Honscheid, K., Huehnerhoff, J., Jordan, B., Jordan, W. P., Kauffmann, G., Kazin, E. A., Kirkby, D., Klaene, M. A., Kneib, J.-P., Le Goff, J.-M., Lee, K.-G., Long, D. C., Loomis, C. P., Lundgren, B., Lupton, R. H., Maia, M. A. G., Makler, M., Malanushenko, E., Malanushenko, V., Mandelbaum, R., Manera, M., Maraston, C., Margala, D., Masters, K. L., McBride, C. K., McDonald, P., McGreer, I. D., McMahon, R. G., Mena, O., Miralda-Escudé, J., Montero-Dorta, A. D., Montesano, F., Muna, D., Myers, A. D., Naugle, T., Nichol, R. C., Noterdaeme, P., Nuza, S. E., Olmstead, M. D., Oravetz, A., Oravetz, D. J., Owen, R., Padmanabhan, N., Palanque-Delabrouille, N., Pan, K., Parejko, J. K., Pâris, I., Percival, W. J., Pérez-Fournon, I., Pérez-Ràfols, I., Petitjean, P., Pfaffenberger, R., Pforr, J., Pieri, M. M., Prada, F., Price-Whelan, A. M., Raddick, M. J., Rebolo, R., Rich, J., Richards, G. T., Rockosi, C. M., Roe, N. A., Ross, A. J., Ross, N. P., Rossi, G., Rubiño-Martin, J. A., Samushia, L., Sánchez, A. G., Sayres, C., Schmidt, S. J., Schneider, D. P., Scóccola, C. G., Seo, H.-J., Shelden, A., Sheldon,

E., Shen, Y., Shu, Y., Slosar, A., Smee, S. A., Snedden, S. A., Stauffer, F., Steele, O., Strauss, M. A., Streblyanska, A., Suzuki, N., Swanson, M. E. C., Tal, T., Tanaka, M., Thomas, D., Tinker, J. L., Tojeiro, R., Tremonti, C. A., Vargas Magaña, M., Verde, L., Viel, M., Wake, D. A., Watson, M., Weaver, B. A., Weinberg, D. H., Weiner, B. J., West, A. A., White, M., Wood-Vasey, W. M., Yeche, C., Zehavi, I., Zhao, G.-B., and Zheng, Z. (2013, January). The Baryon Oscillation Spectroscopic Survey of SDSS-III. Astron. J. , **145**, 10.

de Jong, R. S., Bellido-Tirado, O., Chiappini, C., Depagne, É., Haynes, R., Johl, D., Schnurr, O., Schwope, A., Walcher, J., Dionies, F., Haynes, D., Kelz, A., Kitaura, F. S., Lamer, G., Minchev, I., Müller, V., Nuza, S. E., Olaya, J.-C., Piffl, T., Popow, E., Steinmetz, M., Ural, U., Williams, M., Winkler, R., Wisotzki, L., Ansorge, W. R., Banerji, M., Gonzalez Solares, E., Irwin, M., Kennicutt, R. C., King, D., McMahon, R. G., Koposov, S., Parry, I. R., Sun, D., Walton, N. A., Finger, G., Iwert, O., Krumpe, M., Lizon, J.-L., Vincenzo, M., Amans, J.-P., Bonifacio, P., Cohen, M., Francois, P., Jagourel, P., Mignot, S. B., Royer, F., Sartoretti, P., Bender, R., Grupp, F., Hess, H.-J., Lang-Bardl, F., Muschielok, B., Böhringer, H., Boller, T., Bongiorno, A., Brusa, M., Dwelly, T., Merloni, A., Nandra, K., Salvato, M., Pragt, J. H., Navarro, R., Gerlofsma, G., Roelfsema, R., Dalton, G. B., Middleton, K. F., Tosh, I. A., Boeche, C., Caffau, E., Christlieb, N., Grebel, E. K., Hansen, C., Koch, A., Ludwig, H.-G., Quirrenbach, A., Sbordone, L., Seifert, W., Thimm, G., Trifonov, T., Helmi, A., Trager, S. C., Feltzing, S., Korn, A., and Boland, W. (2012, September). 4MOST: 4-metre multi-object spectroscopic telescope. In *Society of Photo-Optical Instrumentation Engineers (SPIE) Conference Series*, Volume 8446, Society of Photo-Optical Instrumentation Engineers (SPIE) Conference Series.

Drinkwater, M. J., Jurek, R. J., Blake, C., Woods, D., Pimbblet, K. A., Glazebrook, K., Sharp, R., Pracy, M. B., Brough, S., Colless, M., Couch, W. J., Croom, S. M., Davis, T. M., Forbes, D., Forster, K., Gilbank, D. G., Gladders, M., Jelliffe, B., Jones, N., Li, I.-H., Madore, B., Martin, D. C., Poole, G. B., Small, T., Wisnioski, E., Wyder, T., and Yee, H. K. C. (2010, January). The WiggleZ Dark Energy Survey: survey design and first data release. Mon. Not. R. Astr. Soc. , **401**, 1429–1452.

Eisenstein, D. J. and Hu, W. (1998, March). Baryonic Features in the Matter Transfer Function. Astrophys. J. , **496**, 605.

Eisenstein, D. J., Seo, H.-J., Sirko, E., and Spergel, D. N. (2007*a*, August). Improving Cosmological Distance Measurements by Reconstruction of the Baryon Acoustic Peak. Astrophys. J. , **664**, 675–679.

Eisenstein, D. J., Seo, H.-J., and White, M. (2007*b*, August). On the Robustness of the Acoustic Scale in the Low-Redshift Clustering of Matter. Astrophys. J. , **664**, 660–674.

Eisenstein, D. J., Weinberg, D. H., Agol, E., Aihara, H., Allende Prieto, C., Anderson, S. F., Arns, J. A., Aubourg, É., Bailey, S., Balbinot, E., and et al. (2011, September). SDSS-III: Massive Spectroscopic Surveys of the Distant Universe, the Milky Way, and Extra-Solar Planetary Systems. Astron. J. , **142**, 72.

Feldman, H. A., Kaiser, N., and Peacock, J. A. (1994, May). Power-spectrum analysis of three-dimensional redshift surveys. Astrophys. J. , **426**, 23–37.

Gelman, A. and Rubin, D.B. (1992). Inference from iterative simulation using multiple sequences. *Statistical Science*, **7**, 457–511. http://www.stat.columbia.edu/ gelman/research/published/itsim.pdf.

Giannantonio, T., Ross, A. J., Percival, W. J., Crittenden, R., Bacher, D., Kilbinger, M., Nichol, R., and Weller, J. (2013, March). Improved Primordial Non-Gaussianity Con-

straints from Measurements of Galaxy Clustering and the Integrated Sachs-Wolfe Effect. *ArXiv e-prints*.

Gramann, M. (1993, March). An improved reconstruction method for cosmological density fields. Astrophys. J. , **405**, 449–458.

Greig, B., Komatsu, E., and Wyithe, J. S. B. (2013, May). Cosmology from clustering of Lyα galaxies: breaking non-gravitational Lyα radiative transfer degeneracies using the bispectrum. Mon. Not. R. Astr. Soc. , **431**, 1777–1794.

Hamilton, A. J. S. (2005, March). Power Spectrum Estimation I. Basics. *ArXiv Astrophysics e-prints*.

Hawkins, E., Maddox, S., Cole, S., Lahav, O., Madgwick, D. S., Norberg, P., Peacock, J. A., Baldry, I. K., Baugh, C. M., Bland-Hawthorn, J., Bridges, T., Cannon, R., Colless, M., Collins, C., Couch, W., Dalton, G., De Propris, R., Driver, S. P., Efstathiou, G., Ellis, R. S., Frenk, C. S., Glazebrook, K., Jackson, C., Jones, B., Lewis, I., Lumsden, S., Percival, W., Peterson, B. A., Sutherland, W., and Taylor, K. (2003, November). The 2dF Galaxy Redshift Survey: correlation functions, peculiar velocities and the matter density of the Universe. Mon. Not. R. Astr. Soc. , **346**, 78–96.

Heavens, A. F. and Taylor, A. N. (1995, July). A spherical harmonic analysis of redshift space. Mon. Not. R. Astr. Soc. , **275**, 483–497.

Jenkins, A., Frenk, C. S., White, S. D. M., Colberg, J. M., Cole, S., Evrard, A. E., Couchman, H. M. P., and Yoshida, N. (2001, February). The mass function of dark matter haloes. Mon. Not. R. Astr. Soc. , **321**, 372–384.

Kaiser, N. (1987, July). Clustering in real space and in redshift space. Mon. Not. R. Astr. Soc. , **227**, 1–21.

Kazin, E. A., Sánchez, A. G., and Blanton, M. R. (2012, February). Improving measurements of H(z) and D$_A$ (z) by analysing clustering anisotropies. Mon. Not. R. Astr. Soc. , **419**, 3223–3243.

Kirkby, D., Margala, D., Slosar, A., Bailey, S., Busca, N. G., Delubac, T., Rich, J., Bautista, J. E., Blomqvist, M., Brownstein, J. R., Carithers, B., Croft, R. A. C., Dawson, K. S., Font-Ribera, A., Miralda-Escudé, J., Myers, A. D., Nichol, R. C., Palanque-Delabrouille, N., Pâris, I., Petitjean, P., Rossi, G., Schlegel, D. J., Schneider, D. P., Viel, M., Weinberg, D. H., and Yèche, C. (2013, March). Fitting methods for baryon acoustic oscillations in the Lyman-α forest fluctuations in BOSS data release 9. *J. of Cosmology and Astr. Phys.* , **3**, 24.

Landy, S. D. and Szalay, A. S. (1993, July). Bias and variance of angular correlation functions. Astrophys. J. , **412**, 64–71.

Laureijs, R., Amiaux, J., Arduini, S., Auguères, J. ., Brinchmann, J., Cole, R., Cropper, M., Dabin, C., Duvet, L., Ealet, A., and et al. (2011, October). Euclid Definition Study Report. *ArXiv e-prints*.

Lewis, A. and Bridle, S. (2002, November). Cosmological parameters from CMB and other data: A Monte Carlo approach. Phys. Rev. D , **66**(10), 103511.

Matsubara, T. (2008a, October). Nonlinear perturbation theory with halo bias and redshift-space distortions via the Lagrangian picture. Phys. Rev. D , **78**(8), 083519.

Matsubara, T. (2008b, March). Resumming cosmological perturbations via the Lagrangian picture: One-loop results in real space and in redshift space. Phys. Rev. D , **77**(6), 063530.

McDonald, P. and Seljak, U. (2009, October). How to evade the sample variance limit on measurements of redshift-space distortions. *J. of Cosmology and Astr. Phys.* , **10**, 7.

Mehta, K. T., Seo, H.-J., Eckel, J., Eisenstein, D. J., Metchnik, M., Pinto, P., and Xu, X. (2011, June). Galaxy Bias and Its Effects on the Baryon Acoustic Oscillation Measurements. Astrophys. J. , **734**, 94.

Meiksin, A., White, M., and Peacock, J. A. (1999, April). Baryonic signatures in large-scale structure. Mon. Not. R. Astr. Soc. , **304**, 851–864.

Metropolis, N., Rosenbluth, Arianna W., Rosenbluth, Marshall N., Teller, Augusta H., and Teller, Edward (1953). Equation of state calculations by fast computing machines. *Journal of Chemical Physics*, **21**, 1087–1092.

Noh, Y., White, M., and Padmanabhan, N. (2009, December). Reconstructing baryon oscillations. Phys. Rev. D , **80**(12), 123501.

Nusser, A. and Dekel, A. (1992, June). Tracing large-scale fluctuations back in time. Astrophys. J. , **391**, 443–452.

Padmanabhan, N. and White, M. (2009, September). Calibrating the baryon oscillation ruler for matter and halos. Phys. Rev. D , **80**(6), 063508.

Padmanabhan, N., Xu, X., Eisenstein, D. J., Scalzo, R., Cuesta, A. J., Mehta, K. T., and Kazin, E. (2012, December). A 2 per cent distance to z = 0.35 by reconstructing baryon acoustic oscillations - I. Methods and application to the Sloan Digital Sky Survey. Mon. Not. R. Astr. Soc. , **427**, 2132–2145.

Peacock, J. A. and Smith, R. E. (2000, November). Halo occupation numbers and galaxy bias. Mon. Not. R. Astr. Soc. , **318**, 1144–1156.

Peebles, P. J. E. (1980). *The large-scale structure of the universe.*

Peebles, P. J. E. (1989, September). Tracing galaxy orbits back in time. Astrophys. J. Letter, **344**, L53–L56.

Peebles, P. J. E. (1990, October). The gravitational instability picture and the formation of the Local Group. Astrophys. J. , **362**, 1–13.

Percival, W. J. (2005, December). Cosmological structure formation in a homogeneous dark energy background. Astr. & Astrophys. , **443**, 819–830.

Percival, W. J., Verde, L., and Peacock, J. A. (2004, January). Fourier analysis of luminosity-dependent galaxy clustering. Mon. Not. R. Astr. Soc. , **347**, 645–653.

Percival, W. J. and White, M. (2009, February). Testing cosmological structure formation using redshift-space distortions. Mon. Not. R. Astr. Soc. , **393**, 297–308.

Planck Collaboration, Ade, P. A. R., Aghanim, N., Armitage-Caplan, C., Arnaud, M., Ashdown, M., Atrio-Barandela, F., Aumont, J., Baccigalupi, C., Banday, A. J., and et al. (2013*b*, March). Planck 2013 results. XVI. Cosmological parameters. *ArXiv e-prints*.

Planck Collaboration, Ade, P. A. R., Aghanim, N., Armitage-Caplan, C., Arnaud, M., Ashdown, M., Atrio-Barandela, F., Aumont, J., Baccigalupi, C., Banday, A. J., and et al. (2013*a*, March). Planck 2013 Results. XXIV. Constraints on primordial non-Gaussianity. *ArXiv e-prints*.

Press, W. H. and Schechter, P. (1974, February). Formation of Galaxies and Clusters of Galaxies by Self-Similar Gravitational Condensation. Astrophys. J. , **187**, 425–438.

Reid, B. A., Percival, W. J., Eisenstein, D. J., Verde, L., Spergel, D. N., Skibba, R. A., Bahcall, N. A., Budavari, T., Frieman, J. A., Fukugita, M., Gott, J. R., Gunn, J. E., Ivezić, Ž., Knapp, G. R., Kron, R. G., Lupton, R. H., McKay, T. A., Meiksin, A., Nichol, R. C., Pope, A. C., Schlegel, D. J., Schneider, D. P., Stoughton, C., Strauss, M. A., Szalay, A. S., Tegmark, M., Vogeley, M. S., Weinberg, D. H., York, D. G., and Zehavi, I. (2010, May). Cosmological constraints from the clustering of the Sloan Digital Sky Survey DR7 luminous red galaxies. Mon. Not. R. Astr. Soc. , **404**, 60–85.

Reid, B. A., Samushia, L., White, M., Percival, W. J., Manera, M., Padmanabhan, N., Ross, A. J., Sánchez, A. G., Bailey, S., Bizyaev, D., Bolton, A. S., Brewington, H., Brinkmann, J., Brownstein, J. R., Cuesta, A. J., Eisenstein, D. J., Gunn, J. E., Honscheid, K., Malanushenko, E., Malanushenko, V., Maraston, C., McBride, C. K., Muna, D., Nichol, R. C., Oravetz, D., Pan, K., de Putter, R., Roe, N. A., Ross, N. P., Schlegel, D. J., Schneider, D. P., Seo, H.-J., Shelden, A., Sheldon, E. S., Simmons, A., Skibba, R. A., Snedden, S., Swanson, M. E. C., Thomas, D., Tinker, J., Tojeiro, R., Verde, L., Wake, D. A., Weaver, B. A., Weinberg, D. H., Zehavi, I., and Zhao, G.-B. (2012, November). The clustering of galaxies in the SDSS-III Baryon Oscillation Spectroscopic Survey: measurements of the growth of structure and expansion rate at z = 0.57 from anisotropic clustering. Mon. Not. R. Astr. Soc. , **426**, 2719–2737.

Reid, B. A., Spergel, D. N., and Bode, P. (2009, September). Luminous Red Galaxy Halo Density Field Reconstruction and Application to Large-scale Structure Measurements. Astrophys. J. , **702**, 249–265.

Roberts, G.O. (1996). Markov chain concepts related to sampling algorithms. In *Markov chain Monte Carlo in Practice* (ed. W. Gilks, S. Richardson, and D. Spiegelhalter). Chapman and Hall, London.

Ross, A. J., Ho, S., Cuesta, A. J., Tojeiro, R., Percival, W. J., Wake, D., Masters, K. L., Nichol, R. C., Myers, A. D., de Simoni, F., Seo, H. J., Hernández-Monteagudo, C., Crittenden, R., Blanton, M., Brinkmann, J., da Costa, L. A. N., Guo, H., Kazin, E., Maia, M. A. G., Maraston, C., Padmanabhan, N., Prada, F., Ramos, B., Sanchez, A., Schlafly, E. F., Schlegel, D. J., Schneider, D. P., Skibba, R., Thomas, D., Weaver, B. A., White, M., and Zehavi, I. (2011, October). Ameliorating systematic uncertainties in the angular clustering of galaxies: a study using the SDSS-III. Mon. Not. R. Astr. Soc. , **417**, 1350–1373.

Ross, A. J., Percival, W. J., Sánchez, A. G., Samushia, L., Ho, S., Kazin, E., Manera, M., Reid, B., White, M., Tojeiro, R., McBride, C. K., Xu, X., Wake, D. A., Strauss, M. A., Montesano, F., Swanson, M. E. C., Bailey, S., Bolton, A. S., Dorta, A. M., Eisenstein, D. J., Guo, H., Hamilton, J.-C., Nichol, R. C., Padmanabhan, N., Prada, F., Schlegel, D. J., Magaña, M. V., Zehavi, I., Blanton, M., Bizyaev, D., Brewington, H., Cuesta, A. J., Malanushenko, E., Malanushenko, V., Oravetz, D., Parejko, J., Pan, K., Schneider, D. P., Shelden, A., Simmons, A., Snedden, S., and Zhao, G.-b. (2012, July). The clustering of galaxies in the SDSS-III Baryon Oscillation Spectroscopic Survey: analysis of potential systematics. Mon. Not. R. Astr. Soc. , **424**, 564–590.

Samushia, L., Percival, W. J., and Raccanelli, A. (2012, March). Interpreting large-scale redshift-space distortion measurements. Mon. Not. R. Astr. Soc. , **420**, 2102–2119.

Samushia, L., Reid, B. A., White, M., Percival, W. J., Cuesta, A. J., Lombriser, L., Manera, M., Nichol, R. C., Schneider, D. P., Bizyaev, D., Brewington, H., Malanushenko, E., Malanushenko, V., Oravetz, D., Pan, K., Simmons, A., Shelden, A., Snedden, S., Tinker, J. L., Weaver, B. A., York, D. G., and Zhao, G.-B. (2013, February). The clustering of

galaxies in the SDSS-III DR9 Baryon Oscillation Spectroscopic Survey: testing deviations from Λ and general relativity using anisotropic clustering of galaxies. Mon. Not. R. Astr. Soc. , **429**, 1514–1528.

Schlegel, D., Abdalla, F., Abraham, T., Ahn, C., Allende Prieto, C., Annis, J., Aubourg, E., Azzaro, M., Baltay, S. B. C., Baugh, C., Bebek, C., Becerril, S., Blanton, M., Bolton, A., Bromley, B., Cahn, R., Carton, P. ., Cervantes-Cota, J. L., Chu, Y., Cortes, M., Dawson, K., Dey, A., Dickinson, M., Diehl, H. T., Doel, P., Ealet, A., Edelstein, J., Eppelle, D., Escoffier, S., Evrard, A., Faccioli, L., Frenk, C., Geha, M., Gerdes, D., Gondolo, P., Gonzalez-Arroyo, A., Grossan, B., Heckman, T., Heetderks, H., Ho, S., Honscheid, K., Huterer, D., Ilbert, O., Ivans, I., Jelinsky, P., Jing, Y., Joyce, D., Kennedy, R., Kent, S., Kieda, D., Kim, A., Kim, C., Kneib, J. ., Kong, X., Kosowsky, A., Krishnan, K., Lahav, O., Lampton, M., LeBohec, S., Le Brun, V., Levi, M., Li, C., Liang, M., Lim, H., Lin, W., Linder, E., Lorenzon, W., de la Macorra, A., Magneville, C., Malina, R., Marinoni, C., Martinez, V., Majewski, S., Matheson, T., McCloskey, R., McDonald, P., McKay, T., McMahon, J., Menard, B., Miralda-Escude, J., Modjaz, M., Montero-Dorta, A., Morales, I., Mostek, N., Newman, J., Nichol, R., Nugent, P., Olsen, K., Padmanabhan, N., Palanque-Delabrouille, N., Park, I., Peacock, J., Percival, W., Perlmutter, S., Peroux, C., Petitjean, P., Prada, F., Prieto, E., Prochaska, J., Reil, K., Rockosi, C., Roe, N., Rollinde, E., Roodman, A., Ross, N., Rudnick, G., Ruhlmann-Kleider, V., Sanchez, J., Sawyer, D., Schimd, C., Schubnell, M., Scoccimaro, R., Seljak, U., Seo, H., Sheldon, E., Sholl, M., Shulte-Ladbeck, R., Slosar, A., Smith, D. S., Smoot, G., Springer, W., Stril, A., Szalay, A. S., Tao, C., Tarle, G., Taylor, E., Tilquin, A., Tinker, J., Valdes, F., Wang, J., Wang, T., Weaver, B. A., Weinberg, D., White, M., Wood-Vasey, M., Yang, J., Yeche, X. Y. C., Zakamska, N., Zentner, A., Zhai, C., and Zhang, P. (2011, June). The BigBOSS Experiment. *ArXiv e-prints*.

Seljak, U. (2000, October). Analytic model for galaxy and dark matter clustering. Mon. Not. R. Astr. Soc. , **318**, 203–213.

Seljak, U., Hamaus, N., and Desjacques, V. (2009, August). How to Suppress the Shot Noise in Galaxy Surveys. *Physical Review Letters*, **103**(9), 091303.

Seo, H.-J., Eckel, J., Eisenstein, D. J., Mehta, K., Metchnik, M., Padmanabhan, N., Pinto, P., Takahashi, R., White, M., and Xu, X. (2010, September). High-precision Predictions for the Acoustic Scale in the Nonlinear Regime. Astrophys. J. , **720**, 1650–1667.

Seo, H.-J. and Eisenstein, D. J. (2007, August). Improved Forecasts for the Baryon Acoustic Oscillations and Cosmological Distance Scale. Astrophys. J. , **665**, 14–24.

Sheth, R. K. and Tormen, G. (1999, September). Large-scale bias and the peak background split. Mon. Not. R. Astr. Soc. , **308**, 119–126.

Slosar, A., Iršič, V., Kirkby, D., Bailey, S., Busca, N. G., Delubac, T., Rich, J., Aubourg, É., Bautista, J. E., Bhardwaj, V., Blomqvist, M., Bolton, A. S., Bovy, J., Brownstein, J., Carithers, B., Croft, R. A. C., Dawson, K. S., Font-Ribera, A., Le Goff, J.-M., Ho, S., Honscheid, K., Lee, K.-G., Margala, D., McDonald, P., Medolin, B., Miralda-Escudé, J., Myers, A. D., Nichol, R. C., Noterdaeme, P., Palanque-Delabrouille, N., Pâris, I., Petitjean, P., Pieri, M. M., Piškur, Y., Roe, N. A., Ross, N. P., Rossi, G., Schlegel, D. J., Schneider, D. P., Suzuki, N., Sheldon, E. S., Seljak, U., Viel, M., Weinberg, D. H., and Yèche, C. (2013, April). Measurement of baryon acoustic oscillations in the Lyman-α forest fluctuations in BOSS data release 9. *J. of Cosmology and Astr. Phys.* , **4**, 26.

Takada, M., Ellis, R., Chiba, M., Greene, J. E., Aihara, H., Arimoto, N., Bundy, K., Cohen, J., Doré, O., Graves, G., Gunn, J. E., Heckman, T., Hirata, C., Ho, P., Kneib, J.-P., Le

Fèvre, O., Lin, L., More, S., Murayama, H., Nagao, T., Ouchi, M., Seiffert, M., Silverman, J., Sodré, Jr, L., Spergel, D. N., Strauss, M. A., Sugai, H., Suto, Y., Takami, H., and Wyse, R. (2012, June). Extragalactic Science, Cosmology and Galactic Archaeology with the Subaru Prime Focus Spectrograph (PFS). *ArXiv e-prints*.

Tegmark, M. (1997, November). Measuring Cosmological Parameters with Galaxy Surveys. *Physical Review Letters*, **79**, 3806–3809.

Tegmark, M., Blanton, M. R., Strauss, M. A., Hoyle, F., Schlegel, D., Scoccimarro, R., Vogeley, M. S., Weinberg, D. H., Zehavi, I., Berlind, A., Budavari, T., Connolly, A., Eisenstein, D. J., Finkbeiner, D., Frieman, J. A., Gunn, J. E., Hamilton, A. J. S., Hui, L., Jain, B., Johnston, D., Kent, S., Lin, H., Nakajima, R., Nichol, R. C., Ostriker, J. P., Pope, A., Scranton, R., Seljak, U., Sheth, R. K., Stebbins, A., Szalay, A. S., Szapudi, I., Verde, L., Xu, Y., Annis, J., Bahcall, N. A., Brinkmann, J., Burles, S., Castander, F. J., Csabai, I., Loveday, J., Doi, M., Fukugita, M., Gott, III, J. R., Hennessy, G., Hogg, D. W., Ivezić, Ž., Knapp, G. R., Lamb, D. Q., Lee, B. C., Lupton, R. H., McKay, T. A., Kunszt, P., Munn, J. A., O'Connell, L., Peoples, J., Pier, J. R., Richmond, M., Rockosi, C., Schneider, D. P., Stoughton, C., Tucker, D. L., Vanden Berk, D. E., Yanny, B., York, D. G., and SDSS Collaboration (2004, May). The Three-Dimensional Power Spectrum of Galaxies from the Sloan Digital Sky Survey. Astrophys. J. , **606**, 702–740.

Trotta, R. (2008, March). Bayes in the sky: Bayesian inference and model selection in cosmology. *Contemporary Physics*, **49**, 71–104.

Verde, L., Peiris, H. V., Spergel, D. N., Nolta, M. R., Bennett, C. L., Halpern, M., Hinshaw, G., Jarosik, N., Kogut, A., Limon, M., Meyer, S. S., Page, L., Tucker, G. S., Wollack, E., and Wright, E. L. (2003, September). First-Year Wilkinson Microwave Anisotropy Probe (WMAP) Observations: Parameter Estimation Methodology. Astrophys. J. Suppl. Ser. , **148**, 195–211.

White, M., Song, Y.-S., and Percival, W. J. (2009, August). Forecasting cosmological constraints from redshift surveys. Mon. Not. R. Astr. Soc. , **397**, 1348–1354.

Yamamoto, K., Nakamichi, M., Kamino, A., Bassett, B. A., and Nishioka, H. (2006, February). A Measurement of the Quadrupole Power Spectrum in the Clustering of the 2dF QSO Survey. *PASJ*, **58**, 93–102.

York, D. G., Adelman, J., Anderson, Jr., J. E., Anderson, S. F., Annis, J., Bahcall, N. A., Bakken, J. A., Barkhouser, R., Bastian, S., Berman, E., Boroski, W. N., Bracker, S., Briegel, C., Briggs, J. W., Brinkmann, J., Brunner, R., Burles, S., Carey, L., Carr, M. A., Castander, F. J., Chen, B., Colestock, P. L., Connolly, A. J., Crocker, J. H., Csabai, I., Czarapata, P. C., Davis, J. E., Doi, M., Dombeck, T., Eisenstein, D., Ellman, N., Elms, B. R., Evans, M. L., Fan, X., Federwitz, G. R., Fiscelli, L., Friedman, S., Frieman, J. A., Fukugita, M., Gillespie, B., Gunn, J. E., Gurbani, V. K., de Haas, E., Haldeman, M., Harris, F. H., Hayes, J., Heckman, T. M., Hennessy, G. S., Hindsley, R. B., Holm, S., Holmgren, D. J., Huang, C.-h., Hull, C., Husby, D., Ichikawa, S.-I., Ichikawa, T., Ivezić, Ž., Kent, S., Kim, R. S. J., Kinney, E., Klaene, M., Kleinman, A. N., Kleinman, S., Knapp, G. R., Korienek, J., Kron, R. G., Kunszt, P. Z., Lamb, D. Q., Lee, B., Leger, R. F., Limmongkol, S., Lindenmeyer, C., Long, D. C., Loomis, C., Loveday, J., Lucinio, R., Lupton, R. H., MacKinnon, B., Mannery, E. J., Mantsch, P. M., Margon, B., McGehee, P., McKay, T. A., Meiksin, A., Merelli, A., Monet, D. G., Munn, J. A., Narayanan, V. K., Nash, T., Neilsen, E., Neswold, R., Newberg, H. J., Nichol, R. C., Nicinski, T., Nonino, M., Okada, N., Okamura, S., Ostriker, J. P., Owen, R., Pauls, A. G., Peoples, J., Peterson, R. L., Petravick, D., Pier, J. R., Pope, A., Pordes, R., Prosapio,

A., Rechenmacher, R., Quinn, T. R., Richards, G. T., Richmond, M. W., Rivetta, C. H., Rockosi, C. M., Ruthmansdorfer, K., Sandford, D., Schlegel, D. J., Schneider, D. P., Sekiguchi, M., Sergey, G., Shimasaku, K., Siegmund, W. A., Smee, S., Smith, J. A., Snedden, S., Stone, R., Stoughton, C., Strauss, M. A., Stubbs, C., SubbaRao, M., Szalay, A. S., Szapudi, I., Szokoly, G. P., Thakar, A. R., Tremonti, C., Tucker, D. L., Uomoto, A., Vanden Berk, D., Vogeley, M. S., Waddell, P., Wang, S.-i., Watanabe, M., Weinberg, D. H., Yanny, B., Yasuda, N., and SDSS Collaboration (2000, September). The Sloan Digital Sky Survey: Technical Summary. Astron. J. , **120**, 1579–1587.